MAPPING AND PREDICTING THE IONOSPHERIC EFFECTS TO COMMUNICATION SYSTEMS IN NORTHERN AURORA AREAS USING THE GLOBAL POSITIONING SYSTEM

By

Lingyun Wang

RECOMMENDED:

Advisory Committee Chair

Department Head

APPROVED:

Dean, College of Science, Engineering and Mathematics

Dean of the Graduate School

8-1-02

Date

MAPPING AND PREDICTING THE IONOSPHERIC EFFECTS TO COMMUNICATION SYSTEMS IN NORTHERN AURORA AREAS USING THE GLOBAL POSITIONING SYSTEM

A

THESIS

Presented to the Faculty

of the University of Alaska Fairbanks

in Partial Fulfillment of the requirements

for the Degree of

MASTER OF SCIENCE

By

Lingyun Wang, B.S.

Fairbanks, Alaska

August 2002

ABSTRACT

This thesis focuses on mapping and predicting ionospheric effects to communication systems in northern high latitude areas using GPS (Global Positioning System). The monitoring of ionospheric scintillation and TEC (Total Electron Content) over Fairbanks, Alaska has been achieved by using the GSV4004 GPS Ionospheric Scintillation and TEC Monitor (GISTM), which has been installed on the roof of Duckering Building at UAF since September 2001. The algorithm of acquiring equivalent vertical TEC above Fairbanks from various satellite measurements is given in detail. Both an empirical ionosphere model, IRI, and a physics-based ionosphere model, PIM, are used to verify the TEC real field measurement. Another signal estimation method, BP neural network, is used to forecast the TEC short-term variation, which can give better performance than the other two. The relationships among TEC, amplitude scintillation and phase scintillation are analyzed. Multipath effects and the impact to GPS performance from ionospheric scintillation are discussed. Lastly the TEC and scintillation index mapping around Fairbanks is presented.

TABLE OF CONTENTS

LIST OF FIGURES

LIST OF TABLES

ACKNOWLEDGEMENTS

I would like to express my gratitude for the efforts and dedication from my advisory committee:

Dr. Charles E. Mayer

Dr. William Bristow

Dr. Vikas S. Sonwalkar.

Special thanks to Dr. Robert E. Daniell in Computational Physics, Inc. for the time and advice in installing the PIM model program.

Finally there are many thanks that cannot express in words to my parents for all their love they have had in me.

I. Introduction

The ionosphere, which is an ionized part of the earth's atmosphere between about 60 to 1000 km altitude, can effect the propagation of radio frequency signals compared to free space. Disturbances in the ionospheric F region below 1000 km can disrupt the amplitude and phase of the RF signals. The disturbances in propagation mainly result from irregularities of the ionosphere, which can cause scintillations in phase and amplitude to be imposed on the signals received from the satellites. Scintillations are rapid variations in the phase or amplitude of the received signal. For high latitude areas, communication systems also occasionally suffer from magnetic or solar storms. Strong scintillations can lead to degraded performance of communication or navigation systems, such as corrupted navigation output of GPS receivers, and even complete signal loss for the duration of the scintillation activity. The Total Electron Content (TEC) in the signal's propagation path determines the time delay amount due to ionosphere. Monitoring of ionosphere variation can be accomplished by TEC measurement.

There are various ways to measure the TEC value, such as by measuring the amount of Faraday rotation of satellite signal beacons to deduce TEC, or by differential Doppler measurements by Navy Navigation Satellite System (NNSS), GPS and Global Navigation Satellite System (GLONASS), etc. However, due to its wide usage and easy availability, the dual frequency GPS receiver system can provide an easy method to monitor the TEC globally by measurement of the relative phase delay between the two working frequencies L1 and L2. The GPS system described in

this work is capable of measuring not only the number of integrated electrons in the slant GPS signal path, but also signal scintillations.

In this work, the ionospheric monitoring system using GPS receivers is presented in detail both in hardware and software structures, including the GPS signal link budget analysis, source data collecting and parsing process. In order to get the TEC value overhead, the slant TEC measured from various GPS satellites at different elevation angles and azimuth angles are transferred to the equivalent vertical TEC by assumption of a single layer ionosphere. The parsed source data are sorted according to the collecting date and time for offline analysis. For single frequency GPS receivers, the TEC compensation needs to be predicted from ionosphere models.

TEC is the indicator of the ionosphere profile. The GPS receiver described above cannot provide the critical frequency of F2 layer (f_0F2), which is the indicator of the maximum electron density of ionosphere. However, based on the assumption of single slab thickness, f_0F2 can be approximated from the TEC data. From data measurements, the TEC derived f_0F2 shows good agreement with the f_0F2 collected by High Frequency Active Auroral Research Program (HAARP). This provides a way to get f_0F2 by TEC measurement from GPS receivers.

Additionally, the collected TEC data are processed to daily average and monthly average to verify the various widely used ionosphere models, such as International Reference Ionosphere (IRI), and Parameterized Ionosphere Model (PIM). IRI is an empirical model whereas the PIM model is a physics-based model. These two models also need the input of the non-ionosphere information to get the TEC estimation. Thereby the quality is largely determined by the estimation accuracy

of those non-ionosphere parameters, such as sun spot number, solar radio flux at 10.7 cm wavelength, and geomagnetic activity index etc. From real data analysis, it is found that due to the internal restriction on the ionosphere profile altitude input of both models, the estimation from them of TEC is not accurate for high latitude areas. Also those two models are not immediately available to be implemented in real-time electrical systems. Thus an estimation method using neural networks without the inputs of those non-ionosphere parameters is proposed and tested by real data. The short-term estimation using neural networks shows better performance than the other two methods by evaluation of the estimation RMS errors.

As for scintillations, the GPS receiver described above is configured to collect both the amplitude index S4 and phase sigma of GPS signals. By data analysis, it is found that the antenna plays an important role on suppressing the amplitude scintillation due to multipath reflections. Both ionospheric irregularities represented by rapid TEC change rate and multipath reflections represented by code carrier divergence measurement are the main sources of the phase scintillations of GPS signals. Also there is not strong correlation between amplitude scintillation and phase scintillation. Finally a map of the TEC measurements around Fairbanks within one day is plotted, which shows TEC intensities along the satellite orbiting tracks.

From the work done so far, we can say there is not general consensus of the ionosphere models for high latitude areas. All the current models are under development and to be improved by real data collection. The GPS receiver system described in this work gives us a way to monitor the ionosphere variations and scintillation effects to communication or navigation systems.

II. Principle of Global Positioning System and Literature Review of Ionospheric Effects

Before heading to the issue of the research, it is necessary to know the basic working principles of GPS in order to make an analysis of ionospheric effects in detail.

GPS is funded by and controlled by the U. S. Department of Defense (DOD). While there are millions of civilian users of GPS worldwide, the system was initially designed for and is operated by the U. S. military. On midnight May 1, 2000, the SA (Selective Availability, artificially deteriorating the satellite clocks) was set to be zero. But the Precision P(Y) code is still encrypted and reserved for military use on both L1 (1575.42 MHz) and L2 (1227.6 MHz) signals.

GPS provides specially coded satellite signals that can be processed in a GPS receiver, enabling the receiver to compute position, velocity and time (PVT). Four GPS satellite signals are enough in principle to compute positions in three dimensions and the time offset in the receiver clock.

GPS satellites provide a convenient way to measure TEC through its all day and all weather passive navigating signals, which cover most of the places of the earth except the north and south poles (see plotting result in Appendix A). In principle GPS could be used with a receiver network to measure TEC world wide in real time.

A. Working Principle of Global Positioning System

GPS employs TOA (time of arrival) ranging for user position determination. From the time delay and the speed of transmission, we can get range values through

TOA. By making TOA measurements to multiple satellites, three-dimensional positioning is achieved. TOA measurements are not perfect due to errors from atmospheric effects, especially the ionosphere, imperfect clock offset from the time base, and interference of other sources.

1. GPS System Segments

GPS is comprised of three segments: satellite constellation (as shown Figure 2.1), ground control/monitoring network, and user receiving equipment. The satellite constellation segment contains the satellites in orbit that provide the ranging signals and data messages to the user equipment. The operational control segment (OCS) tracks and maintains the satellites in space. The OCS updates the satellite clock corrections and ephemerides as well as numerous other parameters essential to determining user PVT. Lastly, the user receiver equipment performs the navigation, timing, or other related functions.

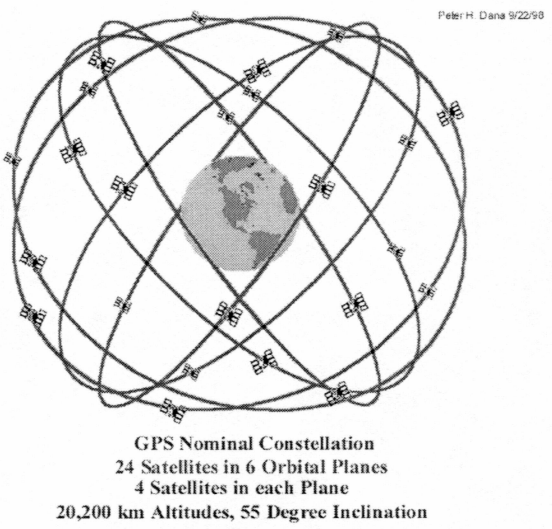

Figure 2.1 GPS satellite constellation. *Peter H. Dana, The Geographer's Craft Project, Department of Geography, The University of Colorado at Boulder.*

The nominal GPS Operational Constellation consists of 24 satellites that orbit the earth in 12 hours. There are often more than 24 operational satellites as new ones are launched to replace older satellites. The satellite orbits repeat almost the same ground track (as the earth turns beneath them) once each day. The orbit altitude of 20,200 km is such that the satellites repeat the same track and configuration over any point approximately every 24 hours (4 minutes earlier each day). There are six orbital planes (with nominally four Space Vehicles (SVs) in each), equally spaced (60 degrees apart), and inclined at about 55 degrees with respect to the equatorial plane. This constellation provides the user with between five and eight SVs visible from any point on the earth.

2. GPS Signal Frequencies and Modulation Format

Figure 2.2 shows the generation process of the generic GPS signal components. Each GPS satellite corresponds to one individual PRN (Pseudo Random Number) number ranging from 1 to 31, which broadcasts two types of PRN ranging codes: a "short" coarse/acquisition (C/A) code and a "long" precision (P) code utilizing direct sequence spread spectrum (DSSS) modulation method. The C/A code has a 1-msec period and repeats constantly, whereas the P code is a 7-day sequence that repeats every midnight Saturday/Sunday.

A block diagram of the SV signal generation process for L1 ($154\ f_0$) and L2 ($120\ f_0$) is shown in Figure 2.2. The L1 frequency (1575.42 MHz) carries the navigation message and the SPS (Standard Positioning Service) code signals.

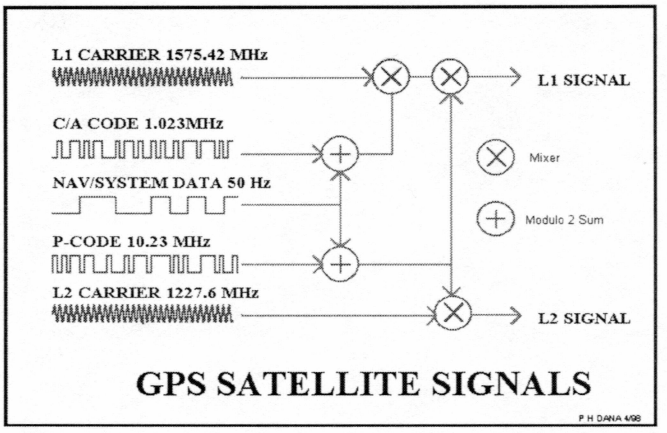

Figure 2.2 Generic GPS satellite signals generation block. *Peter H. Dana, The Geographer's Craft Project, Department of Geography, The University of Colorado at Boulder.*

The L2 frequency (1227.60 MHz) is used to measure the ionospheric delay by PPS (Precise Positioning Services) equipped receivers. PPS users can use two frequencies to measure the ionosphere delay since this delay is related by a scale factor to the difference in signal time of arrival (TOA) for the two carrier frequencies. Single frequency (L1 only) users (SPS users) must estimate the ionospheric delay using modeling parameters that are broadcast to the user in the navigation message.

As shown in the Figure 2.3, the L1 frequency ($154\, f_0$) is modulated by two PRN codes (plus the navigation message data), the coarse/acquisition code (C/A-code), and the precision code (P(Y)-code). The precision code can be denied to SPS users if the control segment activates an Anti-Spoofing (AS) mode in the SV. AS denies access to the P-code by SPS users. Note in Figure 2.2 that the 50 bits per second (bps) data is combined with both the C/A code and the P(Y) code prior to modulation with the L1 carrier. Also note that BPSK modulation is used.

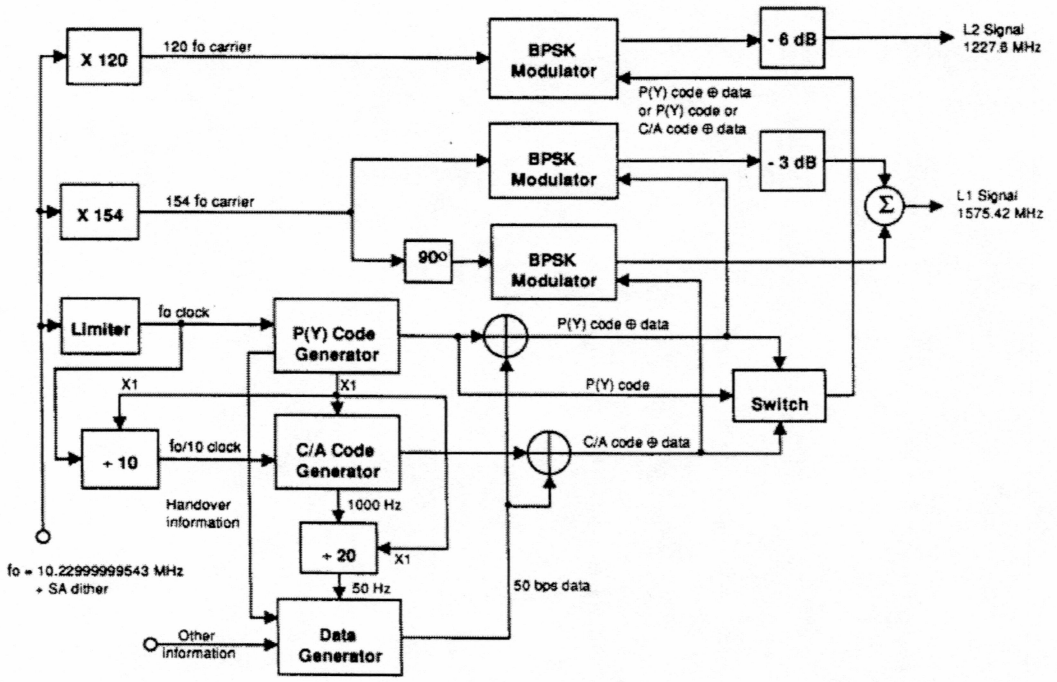

Figure 2.3 GPS satellite signal generation block. From Figure 4.1 of reference 9.

This 50 bps data contains the information required by the receiver to determine following [3]:

1. Satellite time of transmission
2. Satellite position
3. Satellite health
4. Satellite clock correction
5. Propagation delay effects
6. Time transfer to UTC

.

B. Principle of TEC Measurement by GPS

The operating frequency chosen by GPS avoids the specific attenuation due to atmospheric gases such as H_2O and O_2. Also the time delay of GPS due the troposphere does not change rapidly in absolute value, whereas the time delay due to the ionosphere frequently changes by a factor of 10 or more in a single day. It is necessary to know the ionospheric effects on GPS.

The ionosphere is weakly ionized plasma lying in the upper atmosphere, which is created by solar EUV (Extreme Ultraviolet Radiation) ionization of the neutral atmospheric constituents. The electron density of the ionosphere is largely determined by ultraviolet radiation from the Sun. According to the different height and densities of ions, the ionosphere is generally divided into four regions: D, E, F1 and F2.

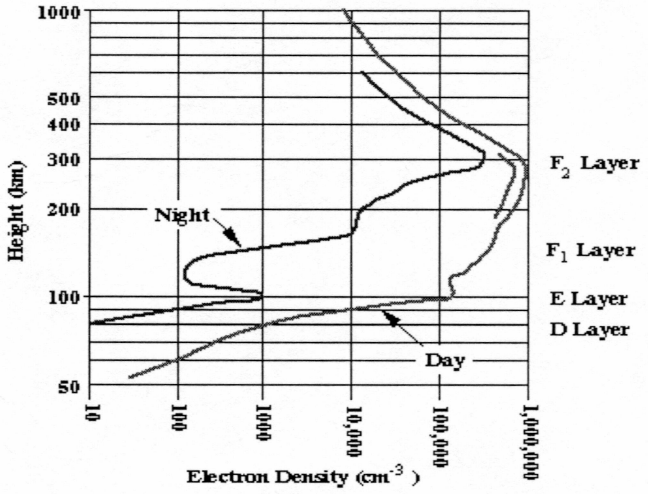

Figure 2.4 Electron Density of the different regions of the ionosphere vs height for day and night time conditions [6]. *From webpage of HAARP.* *http://www.haarp.alaska.edu/haarp/ion4.html*

The F2 layer still exists at night with a lower ion density and greater height compared to daytime [13]. From analysis by J. A. Klobuchar [13], the D region has no

measurable effect on GPS frequencies. The E region is characterized by a normal daily variation, and sporadic layer. It may cause minor scintillation effects with only negligible effects on GPS frequencies. The F2 region is the most variable layer, and also the layer with the maximum density. Its height varies from 200 km to 400 km, and it is generated by ionization of atomic oxygen.

The ionosphere is a dispersive medium, and its refraction index n is a function of operating frequency, whose first order form can be expressed by equation 2.1 [13]

$$n = 1 - \frac{N \cdot e^2}{2 \cdot \varepsilon_0 \cdot m \cdot \varpi^2} = 1 - \frac{f_n^2}{2f^2} \tag{2.1}$$

where N is the electron density, e is the electron charge, -1.602×10^{-19} C, ε_o is the free space permittivity, m is the mass of one electron which is 9.107×10^{-31} kg, ϖ is the operating frequency in radian, f is the operating frequency, and f_n is the critical plasma frequency.

1. Absolute TEC Measurement by Group Delay of the Signal and GPS Range Error

The additional group delay due to the ionosphere can be obtained from the integral of the refractive index of the plasma as in equation 2.2 [13]

$$\Delta t = \frac{1}{c}\int (1-n)dl\,. \tag{2.2}$$

Range error due to time delay can be described as below:

$$\Delta r = \Delta t \cdot c = \int (1-n) dl \,. \tag{2.3}$$

This range error must be compensated to the GPS system when it determines the PVT of the receiver. From equation 2.1, this range error is caused by the plasma refractive index, which is determined by the plasma density N. And N reflects the variability of ionosphere. We need to obtain the integration result of equation 2.2 or 2.3. By combining equations 2.1 to 2.3, we get the relationship between TEC and range error,

$$\Delta r = \int (1-(1-\alpha(f))dl = \alpha(f) \cdot \int N dl = \alpha(f) \cdot TEC \tag{2.4}$$

in which $\alpha(f) = \dfrac{e^2}{8\pi^2 \cdot \varepsilon_0 \cdot m \cdot f^2} = \dfrac{40.3}{f^2}$ is a constant determined by the system operating frequency.

However, it is impossible to get the group delay with only one frequency. Fortunately GPS has two working frequencies, which can be used to get differential ionospheric time delay $\delta(\Delta t)$ as below,

$$\delta(\Delta t) = TEC \cdot \frac{\alpha(f_2) - \alpha(f_1)}{c} \tag{2.5}$$

in which $f_1 = L_1 = 1.575.42$ MHz, $f_2 = L_2 = 1227.60$ MHz.

Thus TEC can be obtained from measurement of the group delay difference of GPS signals as below,

$$TEC = \frac{c \cdot \delta(\Delta t)}{\alpha(f_2) - \alpha(f_1)} = 2.854 \times 10^{25} \cdot \delta(\Delta t) \ [\frac{el}{m^2}]. \tag{2.6}$$

If $\delta(\Delta t)$ is in ns, and TEC is in TEC Unit ($TECU = 10^{16}\ [\frac{el}{m^2}]$), then

$$TEC = 2.854 \cdot \delta(\Delta t)\ [TECU]. \tag{2.7}$$

The time delay difference between L_1 and L_2 provides a way to get the measurement of absolute TEC. However, this kind of measuring method is greatly contaminated by multipath and lack of precise information of the differential pseudorange as obtained from GPS satellites [13]. Besides the improvement by the averaging over many samples that can be measured to sub-nanosecond accuracy, the differential carrier phase advance measurement can provide a way to get a very precise measure of changes in TEC as described in a later part.

2. Precise TEC Variation Measurement by Carrier Phase Advance

Based on the time delay expression in (2.2), the phase advance due to the ionosphere can be represented by (2.8)

$$\Delta\phi = 2\pi f \cdot \Delta t = \frac{2\pi \cdot 40.3}{cf} \int Ndl = \frac{8.44 \times 10^{-7}}{f} TEC \ \text{[radians/sec]}. \tag{2.8}$$

The single frequency phase advance is not practical to know because the phase of the GPS satellite and the receiver is not precisely known, due to the unstable phase of oscillator in the receivers. Fortunately, the differential carrier phase advance

can be measured at the receiver by phase comparison for two frequency GPS receivers.

Two operating frequencies can give a differential or relative carrier phase advance, which is shown by (2.9)

$$\delta(\Delta\phi) = \Delta\phi_2 - \Delta\phi_1 = 8.44 \times 10^{-7} TEC \left(\frac{1}{f_2 - f_1} \right) = 0.17985 \times 10^{-16} TEC$$

[radians/sec]. (2.9)

Measurement of the differential carrier phase advance provides another way to obtain the TEC value. However due to ambiguity of the measurement on the number of the differential phase cycles, this kind of measurement can only give the precise changes in the relative TEC [13]. Because the measuring error of absolute TEC is usually less than the variation of TEC, we can combine the absolute TEC by differential group delay measurement and the precise relative TEC changes to obtain the relative accurate TEC value.

The principle of measuring TEC by the GPS Ionospheric Scintillation and TEC Monitor (GISTM) system utilizes the L1 and L2 carrier phase measurement to smooth the pseudorange differences, and multiplies by the appropriate constant to convert the values to TEC Units (TECU).

C. Other Ionosphere Effects

Due to the variation and irregularities of the ionosphere, which are shown in the variation of the TEC values, there are also other effects besides time delay and phase advance, such as the following.

1. Doppler Shift, or Range-rate Error

Doppler shift, also called range-rate error, is caused by rapid changes of TEC in addition to the receiver's motion, which can be represented by the equation below [4]. It is the rate of change of phase due to the change of TEC, as

$$f_D = \frac{1.34\times10^{-7}}{f}\frac{d(TEC)}{dt} \text{ [Hz]}. \tag{2.10}$$

It is shown that rapid variation of TEC can bring phase shift, which can cause a spectral broadening of the signal. For a stationary receiver, an upper limit of rate of TEC change is 0.1×10^{16} [el/m^2] per second [13] can give a frequency shift of 0.085 Hz at L1 and 0.109 Hz at L2. For typical GPS receivers with carrier tracking loop bandwidth of at least a few hertz (for the GISTM receiver the default loop bandwidth is 10 Hz), it is not a serious impact. For the worst case, the Doppler shift due to the ionosphere can only bring range-rate errors of 1.6 cm/m at L1 and 2 cm/m at L2 [13].

Even the geometric motion of rapidly moving receivers, such as aircraft, can give larger Doppler shifts than the ionosphere. It is not necessary to use the diurnal or seasonal models to correct this kind of range error.

2. Faraday rotation

Faraday rotation is the rotation of the wave polarization while propagating through the medium. It has less impact to GPS systems that utilize circular polarization, but has loss effects for linearly polarized satellite systems, which can be predicted and compensated by the TEC measurement by equation [14] (2.11)

$$\phi = \frac{2.36\times10^4}{f^2} B_{av} \cdot TEC \text{ [radians]}, \tag{2.11}$$

in which B_{av} is the earth's average magnetic field in Wb/m^2. Faraday rotation is not a problem to GPS receivers of right hand circular polarization. If the polarization of the receiver is a linear one for maneuverability and simplicity, there will be –3 dB coupling loss, because only one half the energy will be received by the receiver [13].

3. Amplitude Scintillation

Amplitude scintillation is caused by short-time signal fading due to irregularities of scale sizes from several hundred meters to several kilometers in the Earth's ionosphere. Severe amplitude scintillation can cause the signal to fade below the receiver's lock threshold, which makes the receiver lose the lock of certain satellites. The signal strength varies with the local time, geomagnetic activity, sun spot number (SSN) or solar wind, and geometry of the receiver. Usually the equatorial area has severe signal scintillations. They are strong 1 hour after local sunset until local midnight [13]. The electrojet in polar areas can also bring serious amplitude scintillations [14].

The GISTM GPS receiver can measure amplitude scintillation by using index S4. First the signal is detrended through a low-pass filter to get the normalized S4 index, including ambient noise

$$S4 = \sqrt{\frac{\langle P^2 \rangle - \langle P \rangle^2}{\langle P \rangle^2}}. \tag{2.12}$$

The detrending normalized power output of the low-pass filter can be written as [4]

$$P_k = \frac{(NBP - WBP)_k}{(NBP - WBP)_{lpf,k}}. \tag{2.13}$$

NBP and WBP are the Narrow Band and Wide Band Power respectively as follows, measured over the interval every 20 milliseconds,

$$WBP = \sum_{i=1}^{20} I_i^2 + Q_i^2 \quad \text{and} \quad NBP = \left(\sum_{i=1}^{20} I_i^2 \right)^2 + \left(\sum_{i=1}^{20} Q_i^2 \right)^2, \tag{2.14}$$

where I_i and Q_i are the 1 kHz in-phase and quadraphase samples [4].

Then the effects of ambient noise are removed from S4 by prediction of S4 due to ambient noise through signal to noise ratio measurement as,

$$S4 = \sqrt{\frac{\langle P^2 \rangle - \langle P \rangle^2}{\langle P \rangle^2} - \frac{100}{\overline{S/N_0}} \left[1 + \frac{500}{19\overline{S/N_0}} \right]} \tag{2.15}$$

where the latter part inside the root mark is the predicted S4 due to ambient noise by Van Dierentdoncdk et al [8]. The signal to noise ratio in equation (2.15) is the estimate of S/N_0 over 1 minute.

Thus amplitude scintillation can be monitored by measuring the S4 index.

4. Phase Scintillation

Usually phase scintillation occurs at the same time as amplitude scintillation due to small but rapid changes in the electron content of the ionosphere [13]. The random component in severe phase scintillation will spread out the received signal. From equation 2.8, if the TEC change is 0.19 TECU, there will be 1 radian of phase change at L1, and 1 radian of phase change at L2 corresponds 0.15 TECU of TEC change. For a carrier track loop of only 1 Hz, this will very likely lead to loss of lock of the satellite. Severe phase scintillation only occurs at equinox for high-latitude areas [13].

The GISTM GPS receiver measures the standard deviation of detrended phase by using a high pass filter to remove the low frequency effects from the troposphere and satellite and receiver oscillator effects. This is denoted as $\sigma_{\Delta\phi}$ over 1, 3, 10, 30, and 60 second intervals every 60 seconds.

III. Data Collecting System: GSV 4004 GPS Ionospheric Scintillation and TEC Monitor (GISTM)

In this research, the GSV 4004 GPS Ionospheric Scintillation and TEC Monitor (GISTM) was used to collect scintillation and TEC data. GISTM is a specialized GPS receiver configured to collect ionosphere parameters, such as scintillation index and TEC using principles as stated in part II.

A. GISTM Hardware Structure

GISTM is provided by GPS Silicon Valley Company. It contains as a major component the NovAtel EURO4 dual-frequency receiver, which can measure amplitude and phase scintillation from the L1 and L2 frequency GPS signals simultaneously from 11 GPS satellites in view by 22 receiver channels. Two kinds of GPS antennas come with the system, a choke ring antenna (Model NovAtel GPS 503) and a pinwheel antenna (Model NovAtel GPS 600).

1. System Overview

The GSV 4004 GISTM GPS receiver was deployed in the Satellite Communication Lab of the Electrical and Computer Engineering Department of the University of Alaska Fairbanks with the GPS antenna set on the roof of Duckering Building on UAF's campus from September 2001. Figure 3.1 shows the block diagram of GSV 4004 GISTM system structure.

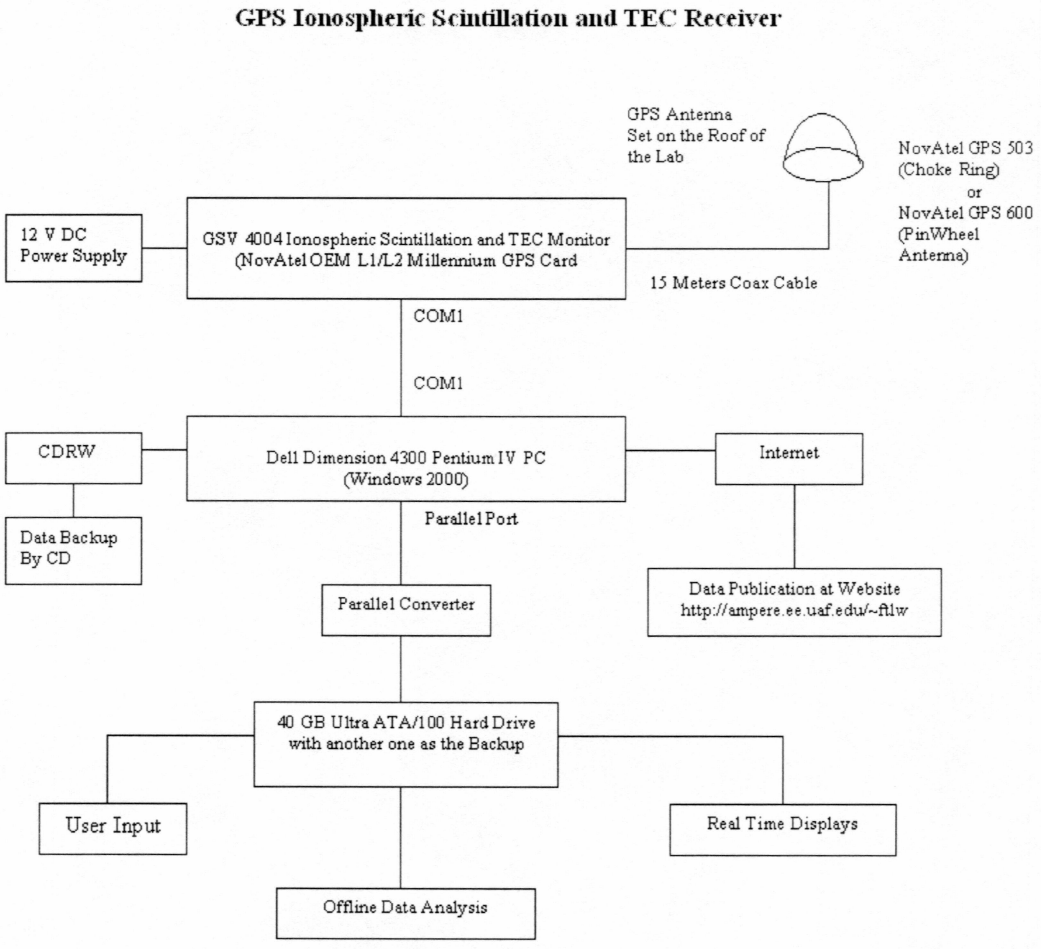

Figure 3.1 Block Diagram of the complete GPS Ionospheric Scintillation and TEC Receiver.

A Dell Dimension 4300 Pentium IV computer running Windows 2000 is used to link and control the GPS receiver through the COM1 port. The receiver is powered by a 12-volt DC power supply. Data are logged onto the hard disk with another hard disk as the backup. The PC communicates with the receiver via the COM1 port, which is a serial communication port. So it is necessary to transform the serial data to parallel data using a parallel converter in the computer. Then the data from the parallel port are recorded to the hard disk under the control of the log configuration

script command. The computer also has a CD-RW to back up the data collected. Using the Internet the data can be accessed from the website: http://ampere.ee.uaf.edu/~ftlw/ (currently still under construction).

The GSV 4004 GPS Ionospheric Scintillation and TEC Receiver in this research is a special version of the NovAtel Euro4 GPS card called the ProPak-4E model, which provides a rugged sealed enclosure for good protection against adverse environments such as northern areas. Also this receiver is different from other types of casual GPS receivers in that it provides three special data log commands to collect signal scintillation data and TEC data by commands RAWSINB, DETRSINB, and ISMRB (where ISMRB is the main data record command), which will be introduced in a later part. Figure 3.2 shows the relationships among the GSV 4004 GPS Ionospheric Scintillation and TEC Receiver, the NovAtel Euro4 GPS, ProPak-4E model and generic GPS receiver.

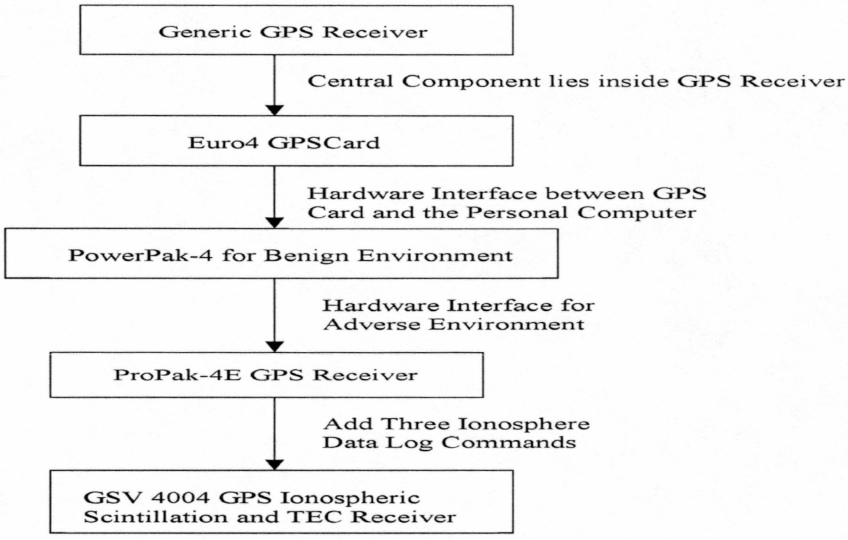

Figure 3.2 Relationships among generic and special configured GPS receivers [15].

NovAtel provided real time software called GPSolution Version 4.2 to monitor the receiver's working status, satellite-locking status, and azimuth and elevation angle display of each satellite. However, GPSolution is only an intuitive monitor tool. It cannot accomplish specific data logging tasks as another script software "**slog,**" that can give an ionospheric data log. In this research GPSolution is used in the initial setup of the receiver, and slog is used in data logging later on.

2. Antenna Setup and Link Budget Analysis

As shown in Figure 3.1, there two kinds of antennas used in different environments. The pinwheel antenna can provide small size and much mobility, but compared to the choke ring antenna, it cannot depress low elevation angle multipath as well. So the choke ring antenna has been installed for data collection, and will be analyzed in the link budget of satellite to ground GPS receiver configuration.

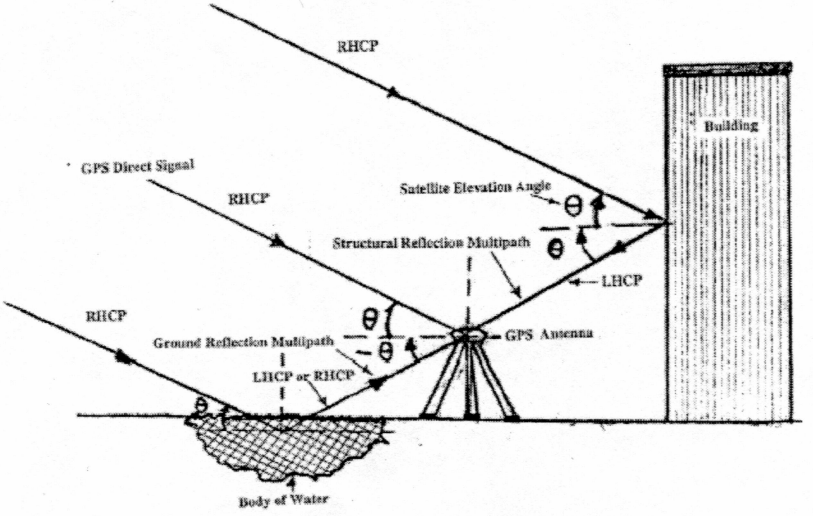

Figure 3.3 Multipath reflections to GPS antenna. (Figure 1 from reference 4)

Figure 3.3 shows multipath signals entering the GPS antenna. Multipath can cause degradation of the signal, especially multipath coming from lower elevation angles. The choke ring antenna uses the principle of cancellation of "primary wave" and "secondary wave" to depress the left hand polarization waves and reflected waves coming from the back of antenna, and keep the direct right hand polarization satellite waves, as shown Figure 3.4. Please refer detail analysis to reference 20.

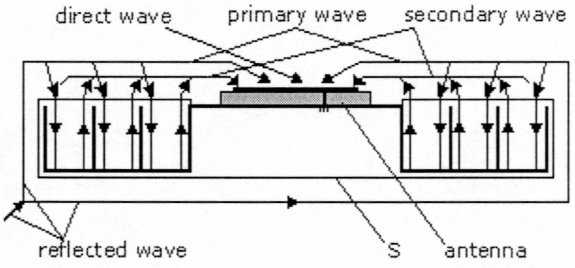

Figure 3.4 Field waves in a choke ring antenna. (From Figure 1 of reference 20.)

Now for a better understanding of carrier to noise ratio measured by the GISTM, it is necessary to analyze the link budget from a satellite to the GPS ground receiver. From the manual of the choke ring antenna used in the research, NovAtel GPS Antenna Model 503, the antenna parameters are shown in Table 3.1.

As specified in ICD-GPS-200 [12], the minimum signal power acceptable by GPS receivers are –158.0 dBW, –162.6 dBW, and –165.2 dBW for L1 C/A, L1 P(Y), and L2 P(Y) codes, respectively. Refer to Table 4.5 in reference 9 for the assumptions of the satellite EIRP, free space loss, and total atmospheric loss.

For example, the minimum received power, S_r, of C/A L1 from GPS BLK II satellites can be obtained like this,

Table 3.1 Electrical specifications of GPSAntenna Model 503 (Choke Ring Antenna). From User Manual of NovAtel L1/L2 GPSAntenna Model 503.

3 dB Pass Band	L1: 1575 ± 10MHz L2: 1227 ± 10MHz
Out-of-band rejection	$f_c \pm 50$MHz: 25 dB (L1), 40 dB (L2) $f_c \pm 100$MHz:45 dB (L1), 40 dB (L2)
Antenna elevation pattern (90°=zenith)	$\theta = 90^\circ$: +8.0 dBic (typical) $20^\circ \le \theta < 90^\circ$: -3.5 dBic to 8.0 dBic (typical) $5^\circ \le \theta < 20^\circ$:-8.5 dBic to –1.0 dBic (typical) $0^\circ \le \theta < 5^\circ$: -9.5 dBic to –5.5 dBic (typical) $\theta = 0^\circ$: -9.5 dBic to –7.0 dBic (typical)
LNA gain	26 ± 2 dB
Polarization	Right-hand Circular
Noise Figure	≤ 2.5 dB
L1-L2 differential propagation delay	≤ 10.0 nsec
Axial Ratio (90°=zenith)	$\theta = 90^\circ$: 2.0 dB max. (L2), 5.0 dB max. (L1) $30^\circ \le \theta < 90^\circ$: 4 .0dB max. (L2), 8.0 dB max (L1) $15^\circ \le \theta < 30^\circ$: 6.0 dB max. (L2), 10.0 dB max. (L1) $5^\circ \le \theta < 15^\circ$: 7.0 dB max. (L2), 11.0 dB max. (L1) $0^\circ \le \theta < 5^\circ$: 6.0 dB max. (L2), 11.0 dB max. (L1)
Nominal Impedance	$50\,\Omega$
VSWR	≤ 2.0:1

$$S_r = P_s + G_{sa} - L_{pm} - L_{at} - L_f + G_{LA} \text{ (dBW)} \tag{3.1}$$

in which

P_s = Power transmitted from the satellite = 13.4 dBW from reference [9]

G_{sa} = Gain of the satellite antenna in the worst case, 13.5 dB

L_{pm} = Loss from polarization mismatch, about 3.4 dB

L_{at} = Loss from atmosphere (mostly from O_2 which is indicated in Figure 3.14 in reference 4), about 2.0 dB

L_f = Free space loss $= \left(\frac{\lambda}{4\pi d} \right)^2$ = 182.5 dB (assume distance from GPS satellite to ground receiver is 20, 200 km)

G_{LA} = Receiver's Linear Antenna Gain, about 3.0 dB.

Thus the minimum received power of C/A L1 at the ground receiver is about −158 dBW. For the received power of other signal components, refer to chapter 4 of reference [9].

So for the C/A L1 signal component, the unjammed C/N_0 at baseband can be given by equation below [9],

$$C/N_0 = S_r + G_a - 10\log(kT_0) - N_f - L \text{ (dB-Hz)} \tag{3.2}$$

in which

S_r = received minimum C/A L1 signal power (dBW), -158 dBW

G_a = antenna gain (dBic) , ranging from –9.5 dBic to +8.0 dBic for GPSAntenna Model 503

$10\log(kT_o)$ = thermal noise density (dBW-Hz) = 204 dBW-Hz

k = Boltzmann constant (watt-sec/K) = 1.38×10^{-23}

T_o = thermal noise reference temperature (K) = 290 K

N_f = noise figure of receiver including antenna and cable losses (dB), less than 2.5 dB for GPSAntenna Model 503.

L = A/D converter loss (dB) assuming for high quality of GISTM, 3 dB

So for different elevation angles of GPS satellites from the ground receiver, the carrier to noise density ranges from 31 dB-Hz to 48.5 dB-Hz.

B. Software and Data Parsing

The first task of this research project is how to collect and extract valuable data from data log files for later data analysis. The structure of the data format should be easy for efficient data programming. Also the file names should be distinct from each other for the easy data recognition of certain days and years.

1. Raw Data Collecting

The NovAtel Euro4 GPS provides a script language called "**slog**" to control and communicate with the receiver by which certain ionosphere parameter data can be logged to the computer's hard disk. For the purpose of monitoring the ionosphere, the GSV 4004 GPS Ionospheric Scintillation and TEC Receiver provides three special data log commands to collect the data of signal scintillation and TEC data by commands RAWSINB, DETRSINB, and ISMRB, of which ISMRB will be introduced in detail.

Figure 3.5 shows the flow chart of the script program configuring the GSV 4004 GISTM Receiver to collect ISMRB data. It is necessary to put one day's data into one distinct file. So the subroutine for time left within a day is used to pause the receiver to collect the data until the end of the day in Universal Time. After that, the program will collect the ISMRB data within one exact day for the other six days in one week. The data file name will be named by the ***found*** command according to time tag. This is useful to sort the data according to time, for later analysis. For the script program list refer to Appendix B.1.

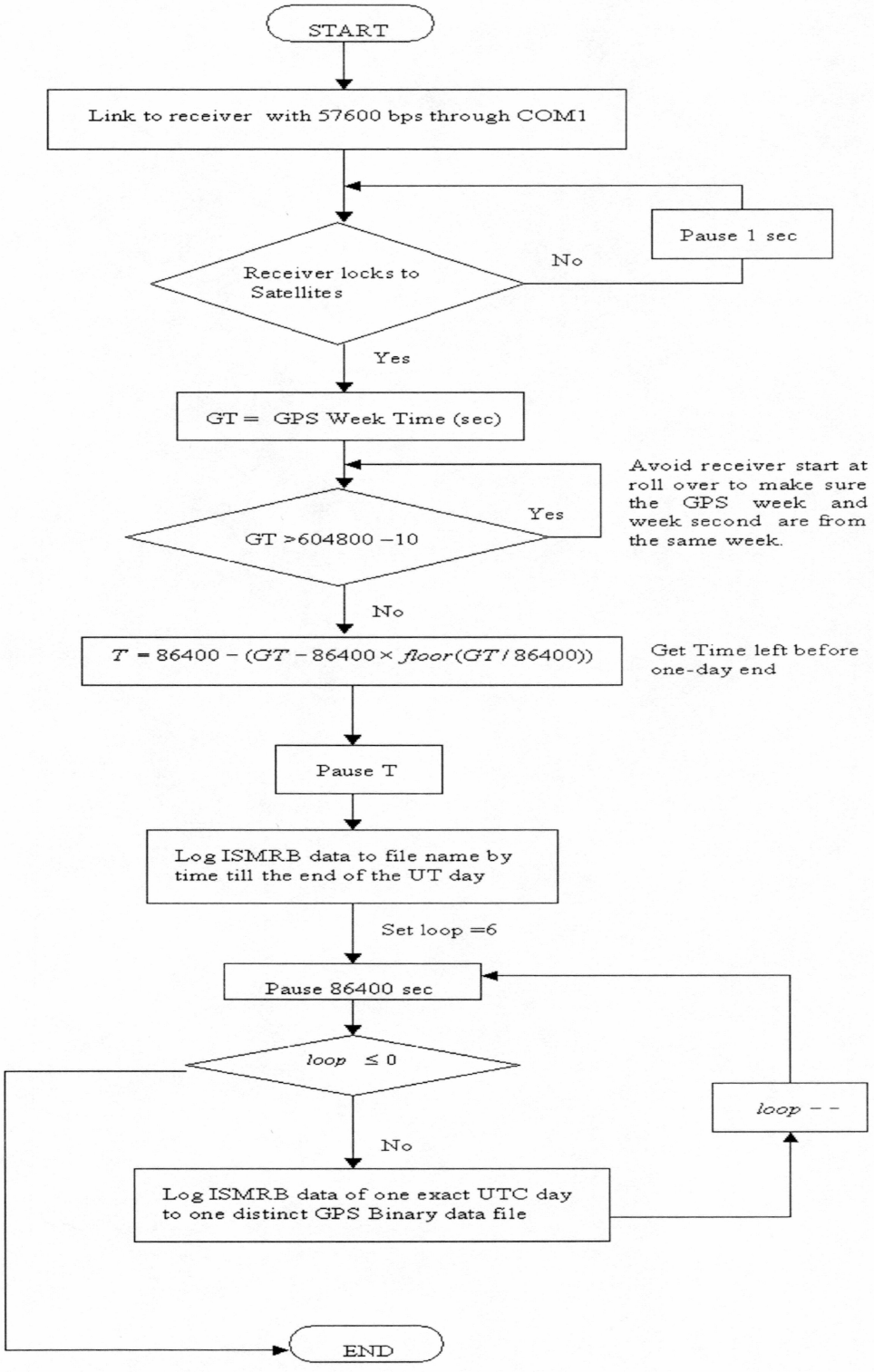

Figure 3.5 Program flow chart for the script program collecting source data.

Table 3.2 Binary data file format collected by data log command ISMRB Adapted from Table III in reference 10.

Field Number	**Data**	**Bytes**	**Format**	**Units**
1	Header	0		N/A
2	Number of SV observed	4	integer	N/A
For first SV observations				
3	PRN	2	integer	N/A
4	SV Azimuth Angle	4	float	degrees
5	SV Elevation Angle	4	float	degrees
6	C/N_o	8	double	dB-Hz
7	S4	8	double	Dimensionless
8	Correction to S4	8	double	Dimensionless
9	1-second phase sigma	8	double	radians
10	3-second phase sigma	8	double	radians
11	10-second phase sigma	8	double	radians
12	30-second phase sigma	8	double	radians
13	60-second phase sigma	8	double	radians
14	Average of Code/Carrier divergence	8	double	meters
15	Sigma of Code/Carrier Divergence	8	double	meters
16	TEC at TOW-45	4	float	TECU
17	ΔTEC from TOW-60 to TOW-45	4	float	TECU
18	TEC at TOW-30	4	float	TECU
19	ΔTEC from TOW-45 to TOW-30	4	float	TECU
20	TEC at TOW-15	4	float	TECU
21	ΔTEC from TOW-30 to TOW-15	4	float	TECU
22	TEC at TOW	4	float	TECU
23	ΔTEC from TOW-15 to TOW	4	float	TECU
24	Lock Time	8	double	seconds
25	Channel status	4	integer	
26	L2 Lock Time	8	double	seconds
27	L2 C/N_o	8	double	seconds
For next SV observations				
..	..	..	..	..

Shown in Table 3.2 is the list of what the ISMRB data log command collects. The format of the data files is binary. The binary data needs to be parsed into text data files using a C++ program.

2. Data Parsing from Binary Source Data Files

After knowing the binary source data format, it is possible to parse the binary data to text format using a C++ program for easy data analysis by other math application software such as Matlab. In Matlab, the text data files can be loaded as a single Matlab matrix. By this data parsing, it is convenient to analyze the ionosphere data needed by simple matrix manipulation.

Data collected by the script program is stored in binary format defined by NovAtel as in Table 3.3.

Table 3.3 Basic format of binary GPS data file [16]

Field Sequence	Binary Data	Format
1	Header	The format is defined by Table 4 in reference 11
2	Data	Format of data collected by script command is defined as in the NovAtel Manual, such as ISMRB in Table3.2
3	CRC	4 bytes

There are three components in the binary GPS data file. The header is used to synchronize the data field and tag the message ID (that is corresponding to one certain script data log command). It also provides the GPS time by GPS week number and week seconds in milliseconds. For details describing of the header structure, refer to Table 4 in reference 16. The structure of data collected by the script command is defined as in the NovAtel user's manual, such as the ISMRB data (the major ionosphere data we desired) in Table 3.2.

From the above information, it is shown that the ISMRB data can be parsed into text data with corresponding GPS time, elevation and azimuth angles, and PRNs of satellites in a single matrix. That is the idea of the C++ parsing program. NovAtel provides an open parse code called *parseismr*. However, it cannot accomplish this matrix data transformation without some necessary changes. The changed code will be a Win 32 executable file.

Figure 3.6 shows the flow chart of the changed parsing program. For the program list, refer to Appendix B.2. The program uses the object oriented programming idea. In the main function, the 31 possible PRNs are requested in a loop order to print the corresponding ionosphere data. The source data file will be opened in read-only manner for 31 times. Also the main function communicates with the Win 32 operating system to save the print out text data into one text data file.

The main function calls the subroutine *ScanforLogs* as shown in Figure 3.6 (a). The *ScanforLogs* subroutine will print out the PRN number, time tag of each data record in a loop manner until the detection of the end of the file. In the *ScanforLogs* subroutine, another subroutine *ParseLog* is called to find the data record corresponding to PRN requested. If the required PRN is found in the ISMR data record, then it will read the ionosphere data and print them out. If not, then all ionosphere data will be allocated zeros and zeros will be printed out. Zeros means at that time the satellite of that PRN is underneath the horizon or is in idle phase or is a bad satellite (unusable PRN). Also a set of data thresholds is set inside this subroutine, such as: the common TEC data cannot exceed 200 TECU, TEC cannot be minus value (sometimes, because of the machine error, it can create some error data of

minus TEC), elevation angle less than certain threshold such as 30^{o} (to remove the big multipath scintillation data at lower elevation angles), and S4 less 1 etc. If any of these thresholds is exceeded, then all data records on that time tag of that PRN will be set to be zero and zeros will be printed out too.

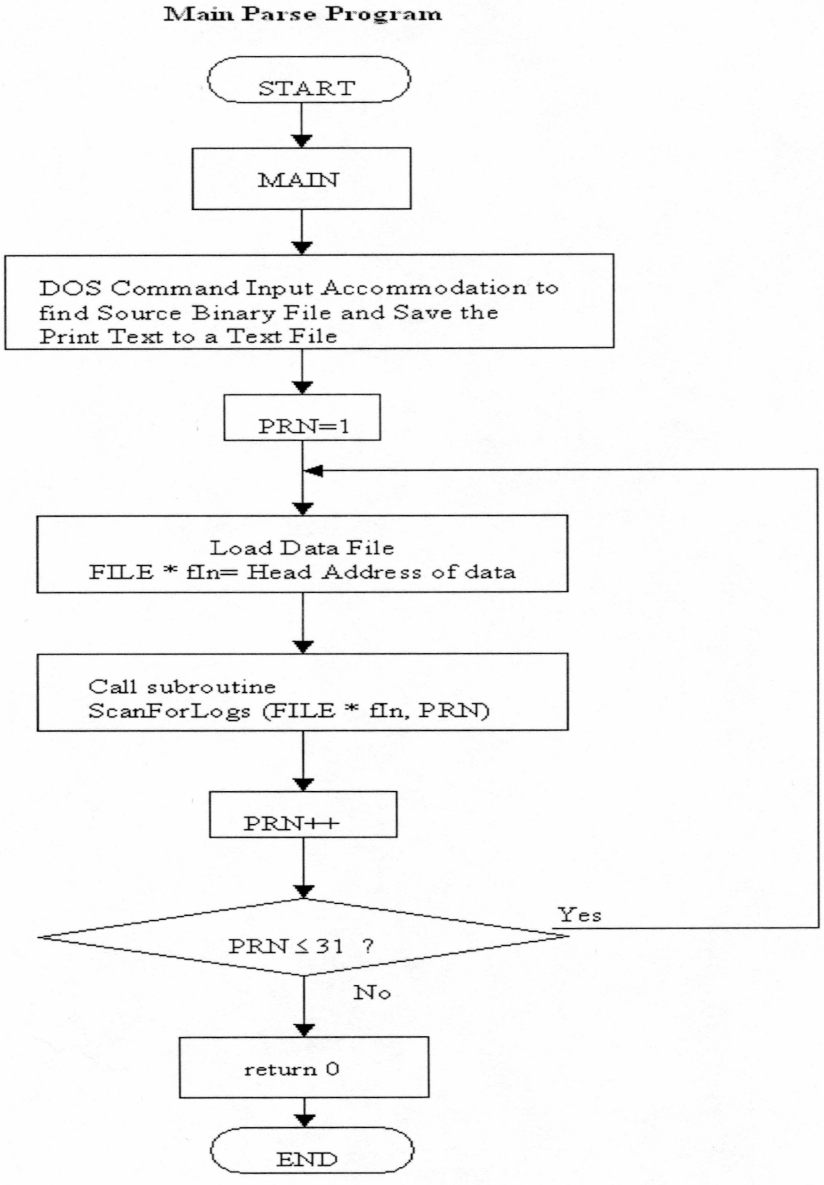

(a)

Subroutine ScanForLogs

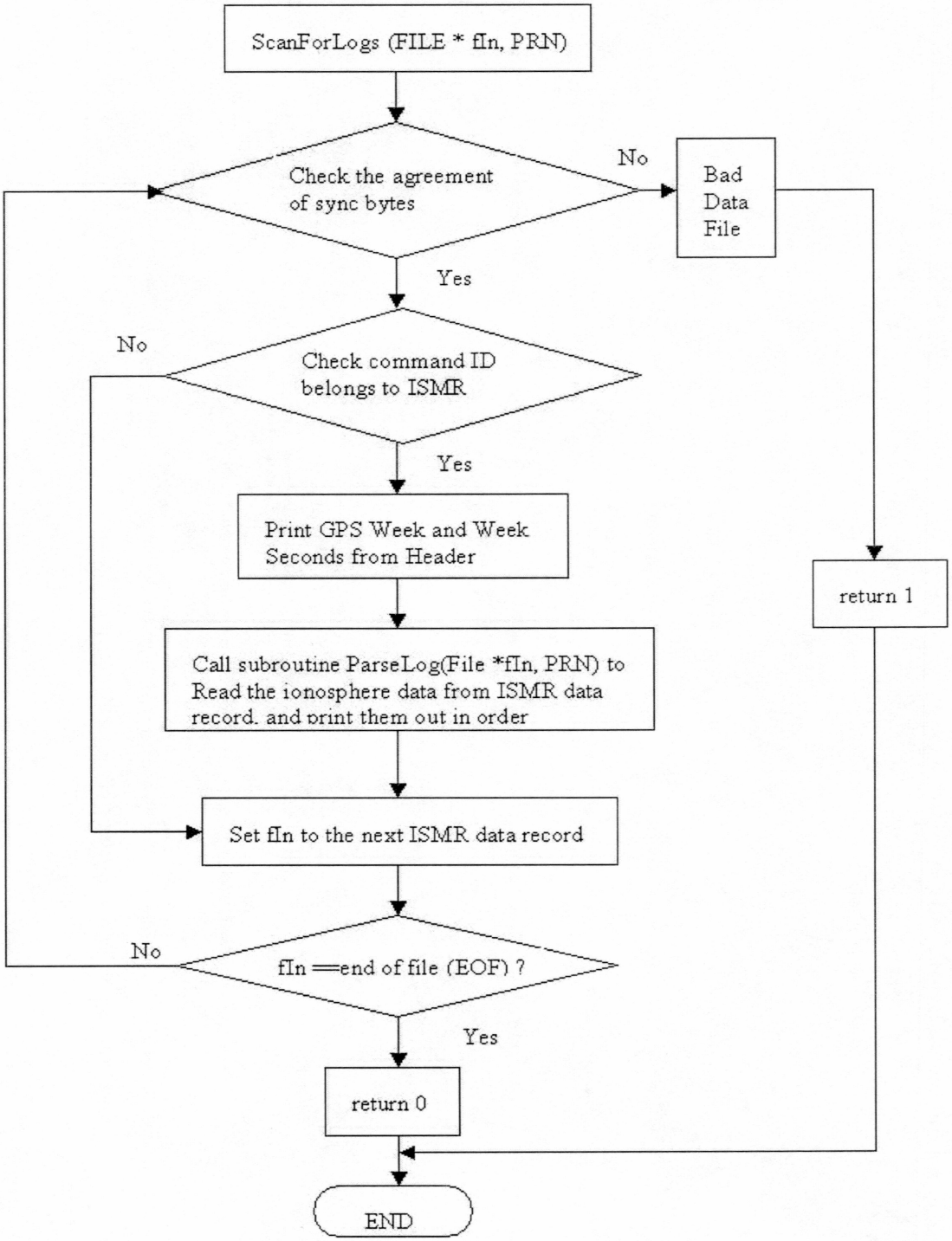

(b)

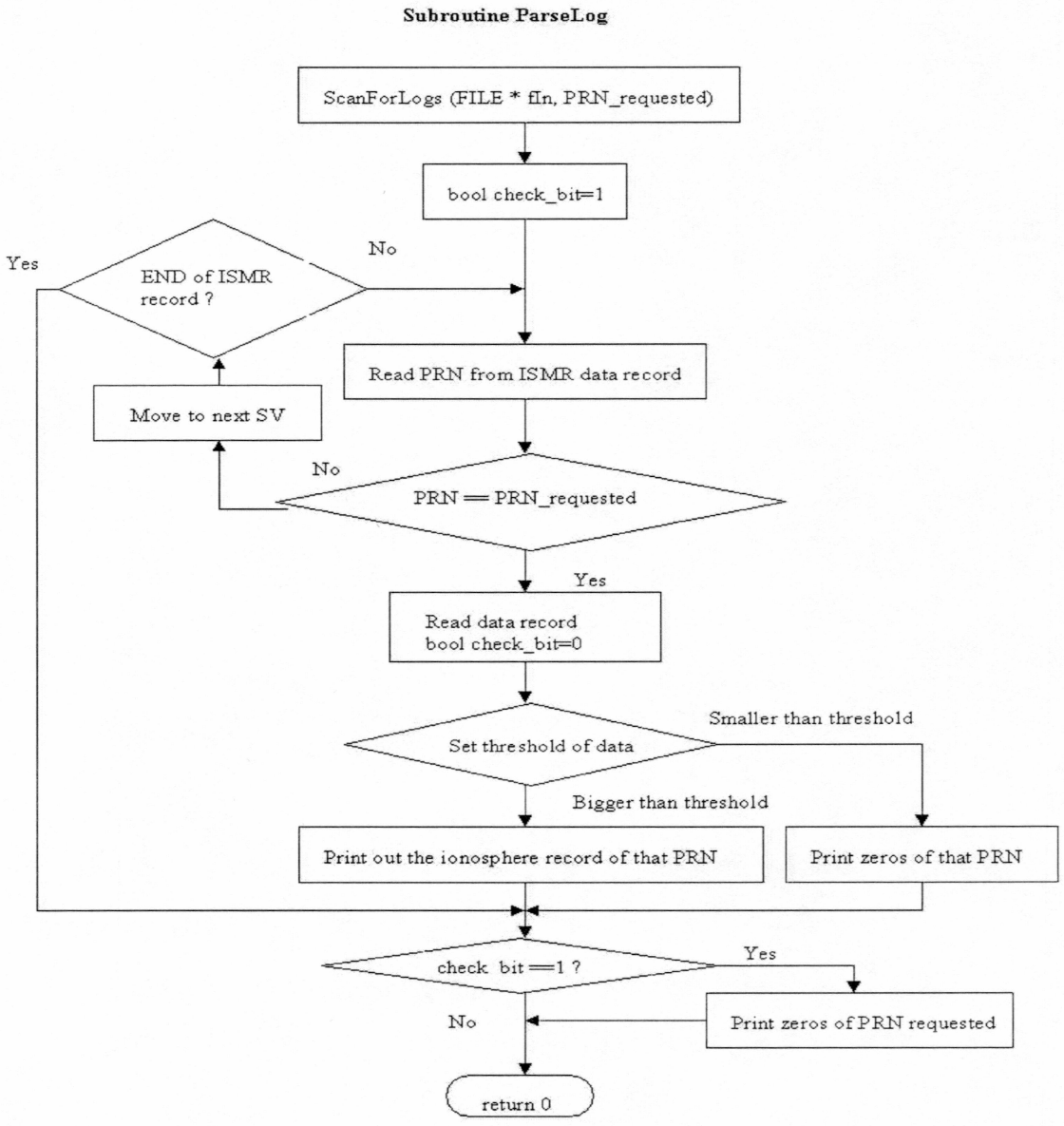

(c)

Figure 3.6 Flow charts for C++ program parsing ISMRB command log data to text data files.

(a) Flow chart for the main parse program.

(b) Flow chart for the subroutine ScanForLogs.

(c) Flow chart for the subroutine of ParseLog.

To save time, a DOS batch file can be created to parse a set of source binary data files. An archive was created for both the source data files and the corresponding parsed text data files according to date of data.

From the parsing process, the source binary data can be changed to a text file with the format shown as below.

Table 3.4 Example of text data format after parsed from binary source file, in which the ISMR is the data record in sequence shown as in Table 3.2 from field number 6 to 27. This is the data on the day of March 20, 2002 with GPS week number 1158, time of the week from 259560 s to 345960, with 1440 data record of each PRN, totally 1440×31 rows.

Week Number	TOW	PRN	Azimuth Angle	Elevation Angle	ISMR Record
1158	259560	1	...	...	... ...
...	...	...	...	...	... ...
1158	345960	1	...	...	... ...
1158	259560	2	...	...	... ...
...	...	...	...	...	... ...
1158	345960	2	...	...	... ...
1158	259560	...	...	...	... ...
...	...	...	...	...	... ...
1158	345960	...	...	...	... ...
1158	259560	31	...	...	... ...
...	...	...	...	...	... ...
1158	345960	31	...	...	... ...

IV. TEC and Scintillation Index Data Analysis

From the above data colleting and parsing process, ISMR data that is GPS ionosphere data listed by Table 3.2, can be loaded to a MatLab matrix. Data from October 30, 2001 to March 18, 2002 was collected using the NovAtel GPS 600 antenna. Data later than March 18, 2002 was collected using the NovAtel GPSAntenna 503. TEC will be modeled and predicted by the RAM, IRI, and PIM models.

A. TEC Data Display

The TEC data parsed from the source data file is actually the slant TEC from the satellite to the ground. It includes not only the ionosphere electron content, but also the electron content of magnetosphere and protonosphere between 2000 km and 20,200 km, the altitude of GPS satellite. In order to get the vertical TEC above one observation station, it is necessary to convert the measured slant TEC to the equivalent vertical TEC. Also an algorithm is provided to extract single site TEC data from multiple satellites at different elevation angles.

1. Conversion of Slant TEC to Equivalent Vertical TEC

Shown in Figure 4.1, the vertical TEC can be inferred by equation 4.1 in terms of elevation angle, earth's radius, and the effective ionospheric height. The ionospheric height is defined as penetration point of the GPS through ionosphere, which is usually assumed to be 400 km [9]. That is the point of the maximum electron content.

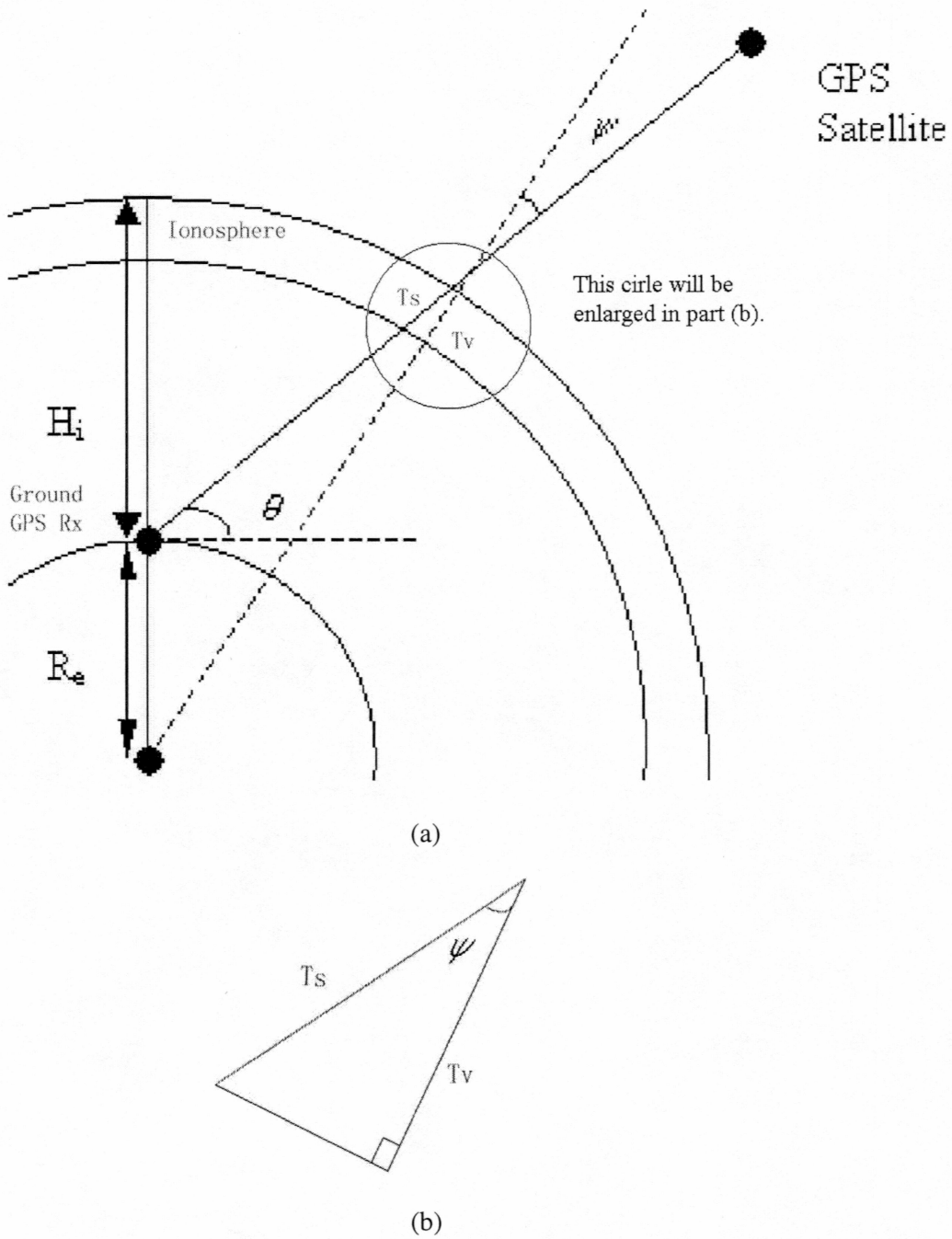

Figure 4.1 Geometry of the transformation from Slant TEC to Vertical TEC.

(a) GPS satellite to receiver link. (b) Enlarged part of circle in (a).

From Figure 4.1(b), the signal length in slant path inside ionosphere is Ts, and the imaginary vertical signal path from the penetration point along the zenith inside the ionosphere is Tv. The electron content in signal path Ts can be transferred to the equivalent electron content in imaginary vertical signal path Tv. The zenith angle of the slant signal path is ψ. Thus the vertical TEC can be represent by equation 4.1.

$$VerticalTEC = SlantTEC \times \cos\psi \tag{4.1}$$

in which ψ can be express as

$$\psi = \arcsin\left(\frac{R_e \cos\theta}{R_e + H_i}\right)$$

where R_e = Earth's radius = 6356.78 km, H_i = effective ionosphere height =350 ~ 400 km, usually chosen as 400 km, and θ = the satellite elevation angle.

This TEC conversion will be used in calculating the approximate TEC above the observation station later on.

2. Calculation Algorithm of TEC Measurement from one single GPS site

What the receiver collects are the TEC data with different elevation angles, different times, and different PRN numbers. Then it is necessary to get vertical TEC from the raw TEC data. In this part, an algorithm of getting a single site TEC will be presented and evaluated.

Figure 4.2 shows a typical receiver collection from PRN #8 within a day. It is shown that without a threshold restriction of elevation angle, the TEC measurement is

strongly interfered with by the low elevation angle multipath scintillation. That is, the lower the elevation angle, the bigger the TEC measurement. The longer transmission distance of the GPS signals inside the atmosphere also causes this poor performance of TEC measurement. From Figure 4.2(b), even after the transformation from slant TEC to vertical TEC, this symptom still exists. It should be noted that the sine wave-like curve in Figure 4.2(b) is caused by the arc sine function inside equation 4.2. So even though the transformation is reasonable by analysis in the above part, it has an internal assumption that the ionosphere is single layer. But in actuality it is not [2]. However, this transformation will still be used in the calculation algorithm later on, which will show reasonable TEC results by processing all PRNs' TEC data.

So from the analysis above, there should be an elevation angle threshold to block out those unreliable data. This angle could not be too large. Otherwise it will cause discontinuity in the TEC measurement. Normally this elevation angle is set to be 30^{o}. That means all the data under this angle will be thrown away. Data above this threshold will be applied to the slant to vertical TEC transformation.

It is necessary to have a method to average the calculated vertical TEC from each available satellite and to insert them according to their time tag, thus getting the measured TEC. Figure 4.3 shows the flow chart of sorting and inserting the source TEC data from all PRNs to the appropriate UTC time, and then averaging them to get real single site TEC.

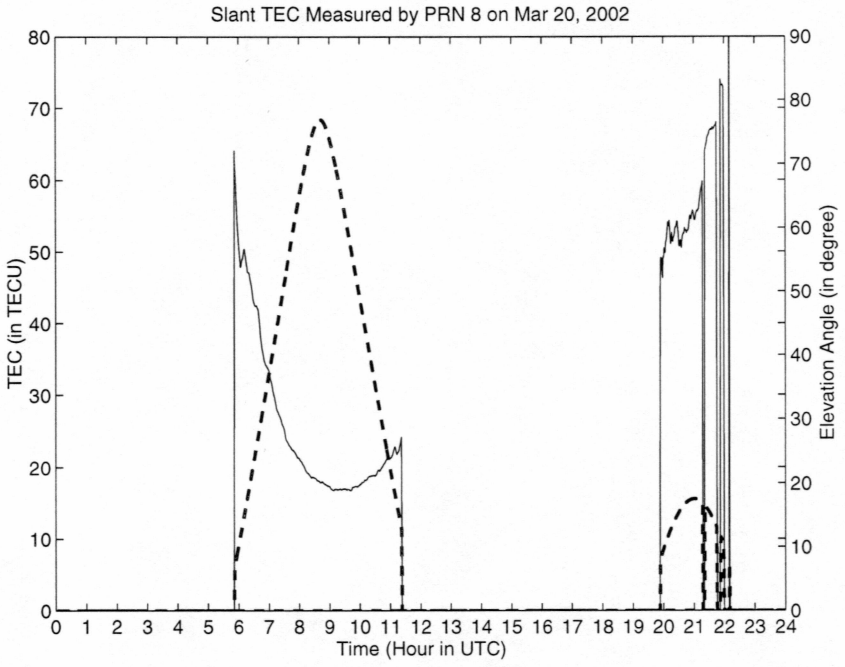

(a)

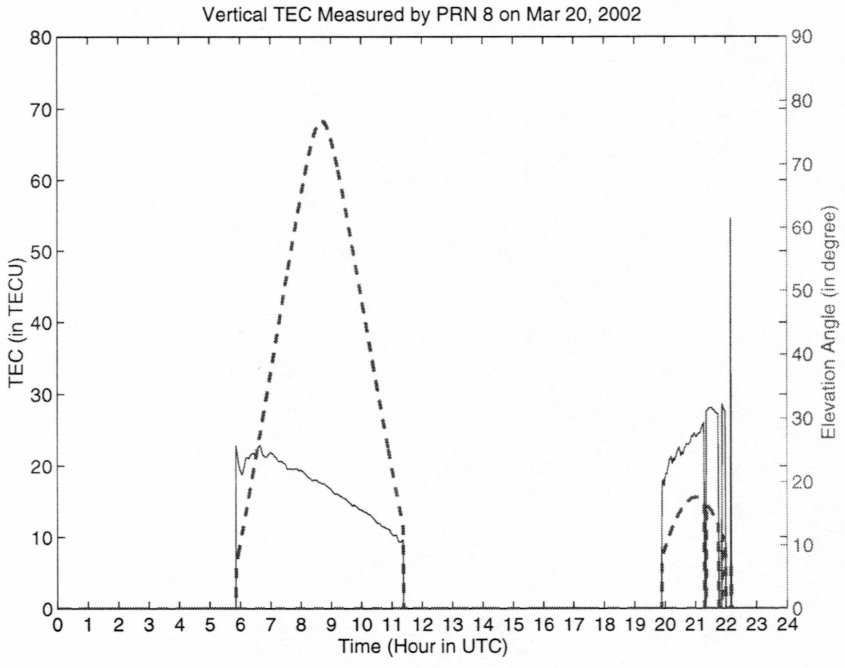

(b)

Figure 4.2 TEC measurement example by PRN 8 on day of Mar 20, 2002

(a) Slant TEC. (b) Equivalent vertical TEC, in which elevation angles are in dashed lines, TEC in solid line.

Without the averaging calculation, the TEC measurement from various PRNs can be plotted as in Figure 4.4, with elevation angles shown below. The elevation angle threshold had been set to be 30^{o}. This can eliminate the burr caused by low angle measurement. After applying the averaging operation outlined in Figure 4.3, the single site TEC can be gotten as shown in Figure 4.5. This is the only method that can provide reasonable TEC measurement above one single GPS site. However this method averages measurements from all parts of the sky, which may have different TEC values, especially if irregularities are present.

The performance of this measurement can be demonstrated by comparing to the data of f_0F2 data from HARRP. This will be shown in a later part by discussing the correlation of TEC and f_0F2.

The error source of vertical TEC measurement comes from measurements with low elevation angles. The 30^{o} elevation angle threshold blocks the poor measurements from low elevation angles from the averaging process, which can reduce the measurement error. Due to the round blank area of the GPS satellite tracks (see Appendix A), the average TEC measurement is about 2^{o} in latitude towards south of Fairbanks, which is incident with the measuring site of the HAARP ionospheric observatory. HAARP is an observatory that includes a high power, high-frequency (HF) radio transmitter for ionospheric research. It is located at Gakona, in South-Central Alaska, about 160 miles southeast to Fairbanks (from HAARP website). So the data from HAARP is very close to those collected at Fairbanks, which can also be shown by the correlation of TEC from Fairbanks and f_0F2 from HAARP.

Algorithm of calculating vertical TEC from various PRN records

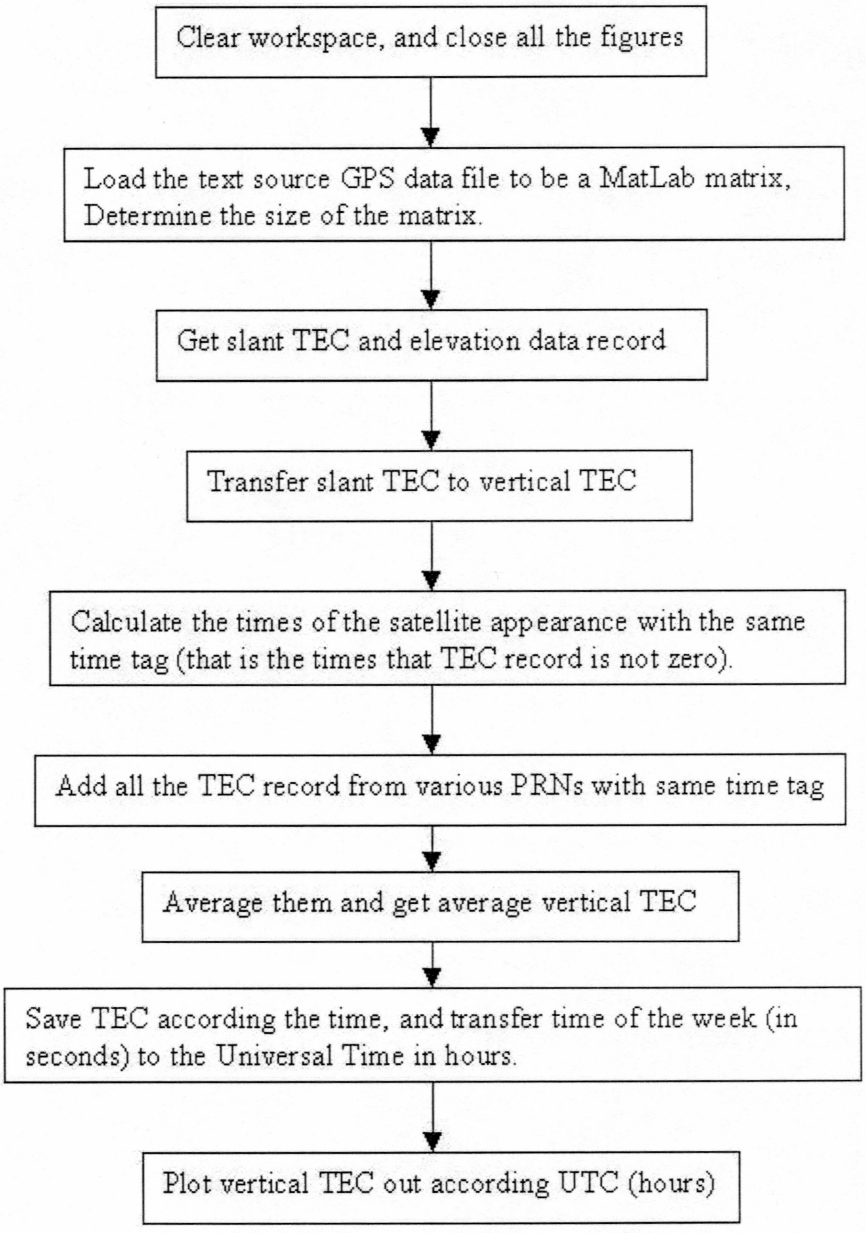

Figure 4.3 Algorithm of calculating vertical TEC from various PRN records. For the program list refer to Appendix B.3. Note: the elevation angles threshold had been set to be 30^{o}.

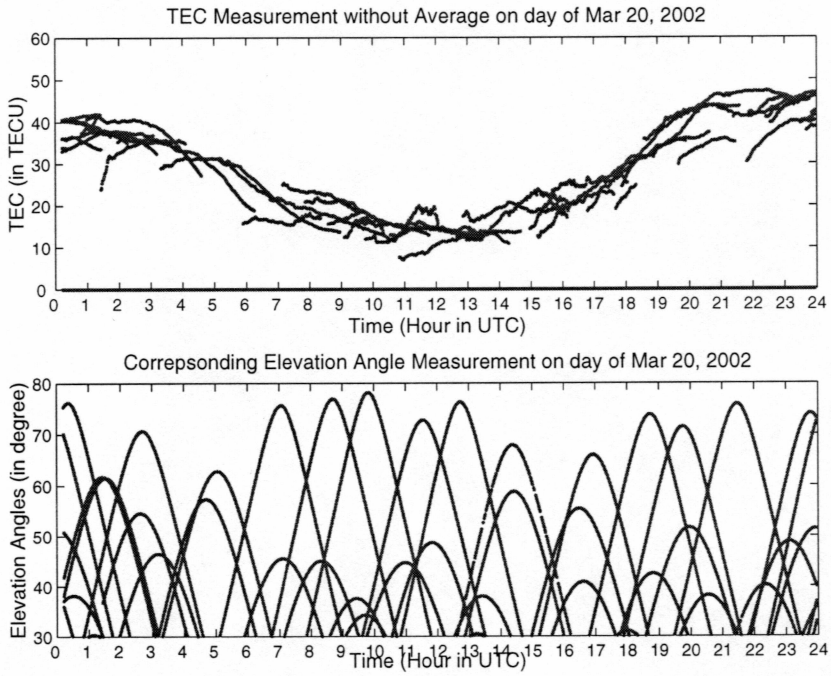

Figure 4.4 TEC measurement from various PRN without averaging on day of Mar 20, 2002, with elevation angles shown below.

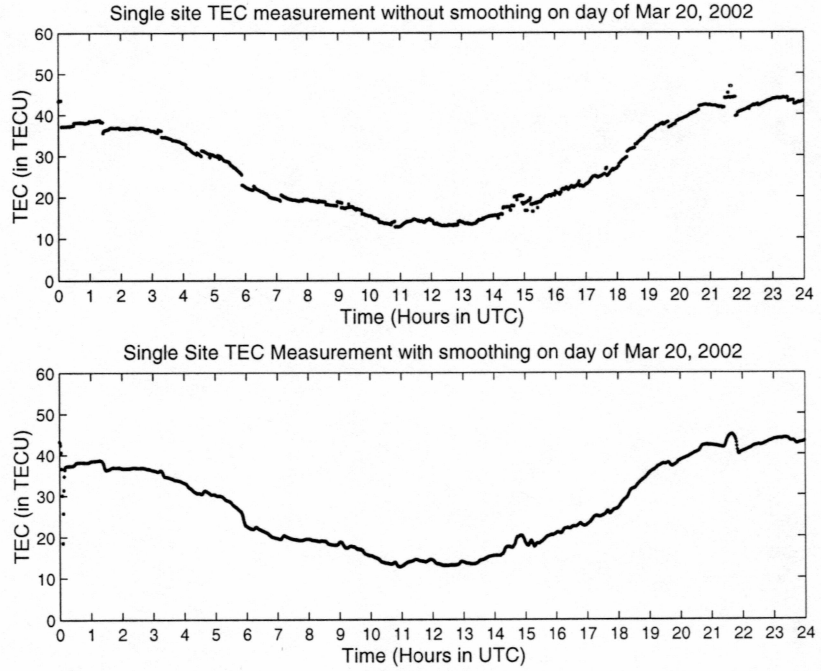

Figure 4.5 Single site TEC measurement above Fairbanks on day of Mar 20, 2002. The Figure above is the unsmoothed measurement while as the Figure below is the smoothed one.

B. Correlation between f_0F2 and TEC

It is meaningful to do correlation work between f_0F2 and TEC, for there are some internal relationships between the two, which can be shown in the theory discussion in part 1 below. The f_0F2 data comes from HAARP measurements at Gakona, which can be downloaded from their website.

1. Deduction of f_0F2 from TEC

From the background literature review, it is clear that the GPS receiver can be configured to get TEC data, which reflects the overall electron content from GPS satellites to the ground receiver, but not the electron density of ionosphere. The f_0F2, critical frequency of the F2 layer, depends on the maximum electron density of the F2 layer, which reflects the fluctuation of peak electron density of the ionosphere. HAARP observatory uses an ionosonde, an instrument that allows direct observation of the ionosphere by high-frequency (HF) radio signals to the upper atmosphere. The F2 layer of the ionosphere is the most variable part of ionosphere contains the maximum electron density of ionosphere, $N_{\max}$. Based on equation 2.1, the maximum electron density determines the upper limit for ordinary model HF vertical propagation that can be reflected back to the earth. This is an important characteristic for short wave radio broadcast, such as VOA (Voice of America), etc.

The ratio of TEC and $N_{\max}$ (also can be regarded as the N_mF2, for the maximum density of ionosphere lies in F2 layer) is defined as slab thickness τ [2]

$$\tau = \frac{TEC}{N_{\max}}. \tag{4.2}$$

From the definition, it is shown that the slab thickness can be regarded as the depth of an imaginary ionosphere with the same TEC but a constant electron density, $N_{\max}$. Since both TEC and $N_{\max}$ vary diurnally, seasonally, geographically, and in response to solar and magnetic activity, it is expected that the slab thickness will not vary much in a short time, such as within one day. However, this is just an assumption. Its variation can show the ionosphere structure profile; such as a high slab thickness value corresponds to 'sharper' peak electron density [2].

How can the $N_{\max}$ in equation 4.2 be determined? From equation 2.1, $N_{\max}$ can be expressed as a function of f_0F2 as below,

$$N_{\max} = \frac{4\pi^2 \varepsilon_o \cdot m}{e^2} \cdot (f_oF2)^2 = 0.0124 \cdot (f_oF2)^2. \tag{4.3}$$

From the work by H. Socicher and Z. Houminer [11], there is a way to determine f_0F2 from TEC measurements by GPS time delay observations. Their result shows that TEC and f_0F2 have similar behavior especially during magnetically active periods. If the slab thickness is assumed to be a constant (this assumption might not be accurate for lower latitude areas, for the ionosphere diurnal variation is very large), such as 483.57 km (this value comes from average TEC = 30 TECU, average f_0F2 = 7 MHz), then the f_0F2 can be approximately deduced from equations (4.2 and 4.3) as below,

$$f_o F2 = \sqrt{\frac{1}{0.0124 \times \tau} TEC} = 1.2782 \times \sqrt{TEC} \ \text{[MHz]} \tag{4.4}$$

in which TEC is in TECU.`

2. Real Field Demonstration Results

From the TEC data, f_0F2 can be approximately obtained. This can be demonstrated from f_0F2 data from HAARP. Shown in Figure 4.6 are the daily TEC measurements at Fairbanks, calculated f_0F2 by equation 4.4, and the corresponding daily f_0F2 measurement by HAARP for two days. The f_0F2 data plot was obtained from the HAARP's website. The ionosonde measurement can give not only the value of f_0F2, but also the corresponding signal reflecting height as shown in the right ordinate.

Due to the restriction of getting the real data from HAARP, it is not possible to precisely calculate the correlation parameter between f_0F2 and TEC. From the plot of Figure 4.6, it is seen that f_0F2 varies in the same manner as TEC. While the variations are similar, there are significant offsets between the two data sets. It should be noted that the difference between the two can be caused by the different measuring sites. So it provides a way to deduce f_0F2 from TEC only if we can get the slab thickness varying information (though it varies very slowly in high latitudes). With slab thickness data calculated by real data, it also can be modeled by the existing slab thickness model as mentioned in reference 11 for northern high latitude areas. Thus accurate f_0F2 can be deduced from TEC measurement.

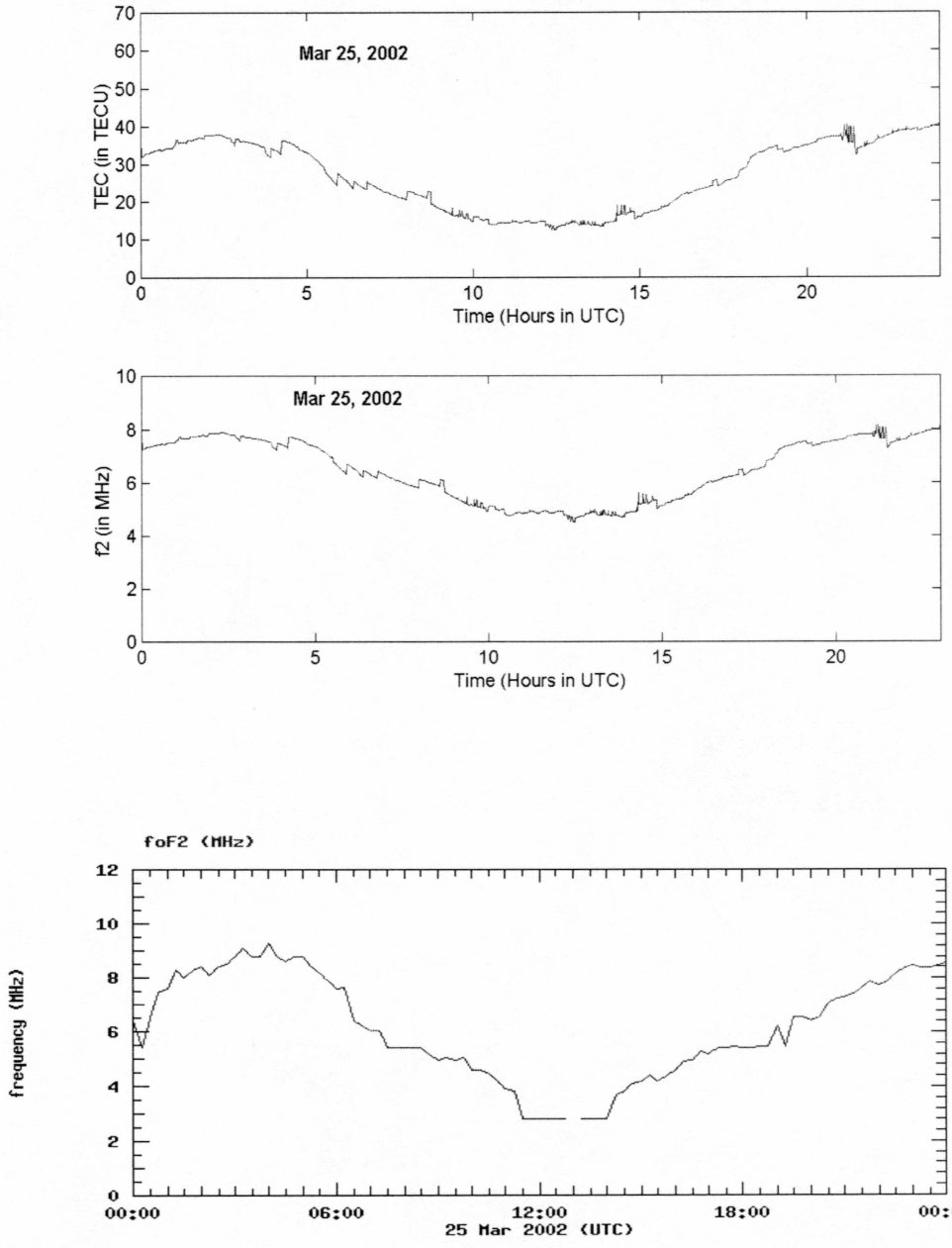
Mar 25, 2002
TEC (in TECU)
Time (Hours in UTC)
Mar 25, 2002
f2 (in MHz)
Time (Hours in UTC)
foF2 (MHz)
frequency (MHz)
height (km)
25 Mar 2002 (UTC)

(a)

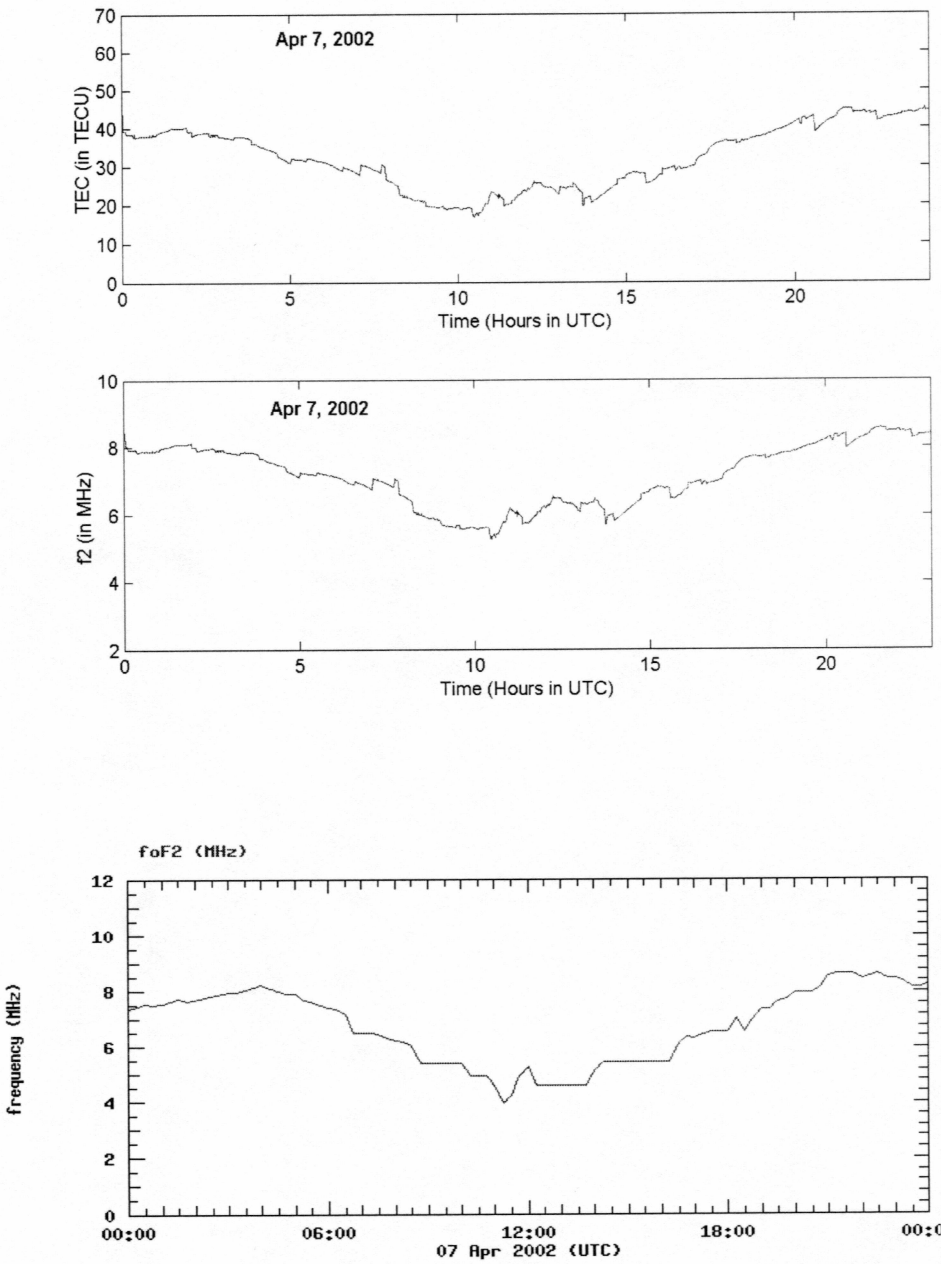

(b)

Figure 4.6 Display of TEC (upper one), calculated f_0F2 (middle one), and corresponding f_0F2 (lower one) from HAARP's website. The f_0F2 data plot comes from the historic data at HAARP's website.

(a) For day March 25, 2002. (b) For day April 7, 2002.

C. TEC Data Analysis

After collecting the ionosphere data for about one year, it is important to analyze the TEC short and long time variation pattern and use ionosphere models IRI and PIM to simulate the variation. Then we will do model verification work and get the comparison results. Using the method of calculating TEC within one day, one month's TEC data can be averaged to one data record with respect to day, hour, and time. Also the data interval of 1 minute can be compressed to 1 hour by an averaging operation. The large data of megabytes order can thus be simplified by easy processing.

1. TEC Short Time Variation Pattern

Shown in Figure 4.7 is TEC versus time (day) from October 29, 2001 to the present. The data plotted are the average TEC points based on 60 TEC collections within one hour. It should be noted that the gaps (points with zero values) were caused by system stoppages and idles, which indicates lack of data, not the real measurements.

It is shown that the diurnal variations in the winter times are much bigger than the summer times. This is caused by the local varying sunset and sunrise time. For a northern high latitude position like Fairbanks, the summer daytime is much longer than wintertime. Thus the number of ions generated by the sun does not vary to as a large degree as in winter. So as reflected in the TEC measurement, the variation of TEC in the summer time is much smaller compared to winter times.

Taking one day for example as shown in Figure 4.5, the maximum TEC appears at about 3 pm (local time), and the minimum TEC appears at about 2 am (local time). That means the ions in the ionosphere move in the sun orbiting direction with about 2 to 3 hours delay in time.

Also observed from Figure 4.7, the maximum TEC values changed from about 80 TECU in October, 2001 to 40 TEC in May, 2002, which reflects the sun spot number changes from high to low. This agrees with the F10.7-derived sunspot numbers dropping down from the 11 year maximum in 2001 provided by North West Research Associates, Inc.

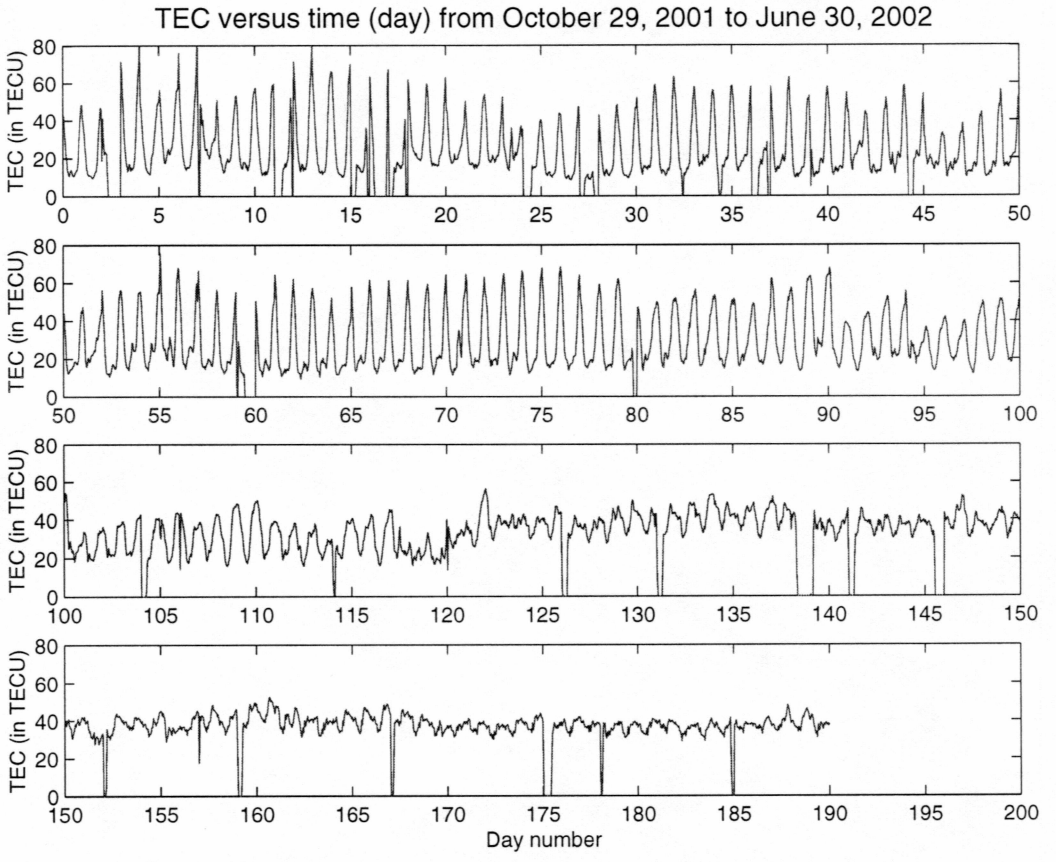

Figure 4.7 TEC versus time (day) from October 29, 2001.

2. TEC Long Time Variation Study

From the long time TEC variation plot as shown in Figure 4.7, the TEC varies with the seasons and the sunspot number. Based on the monthly mean vertical TEC and its standard deviation, T.L. Gulyaeva proposed a Regional Analytical Model (RAM) of ionospheric TEC [19]. The RAM is rather simple in principle, which can give quicker ionosphere prediction on long time scale than sophisticated global models.

In the RAM model, TEC and its standard deviation are functions of the geomagnetic latitude (g), local time (t), seasonal months (s), and solar activity (sunspot number Rz). For the current single site measurement, only t, s, and Rz will be used to verify the model. The RAM model uses the superposition of trigonometric functions as shown below to simulate the TEC and its standard deviation variation.

$$F(x) = \sum C_i \times T_i(x) \tag{4.5}$$

$i = 0,\quad 1, 2, 3$

where $T_0(x) = 1$, $T_1(x) = \sin(x)$, $T_2(x) = \cos(x)$, $T_3(x) = \cos(2x)$. $F(x)$ can be TEC or its standard deviation.

The coefficients of C_i can be determined by temporal and spatial interpolation as below,

$$C_0 = (F(x_0) + F(x_1) + F(x_2) + F(x_3))/4$$

$$C_1 = (F(x_1) - F(x_3))/2$$

$$C_2 = (F(x_0) - F(x_2))/2$$

$$C_3 = (F(x_0) + F(x_2) - F(x_1) - F(x_3))/4 . \quad (4.6)$$

The input variable t can be set as the selected 4 values from 24 hour TEC measurements by $x = t \times 15^\circ \quad t = 0,1,...,23\,\mathrm{UT}$.

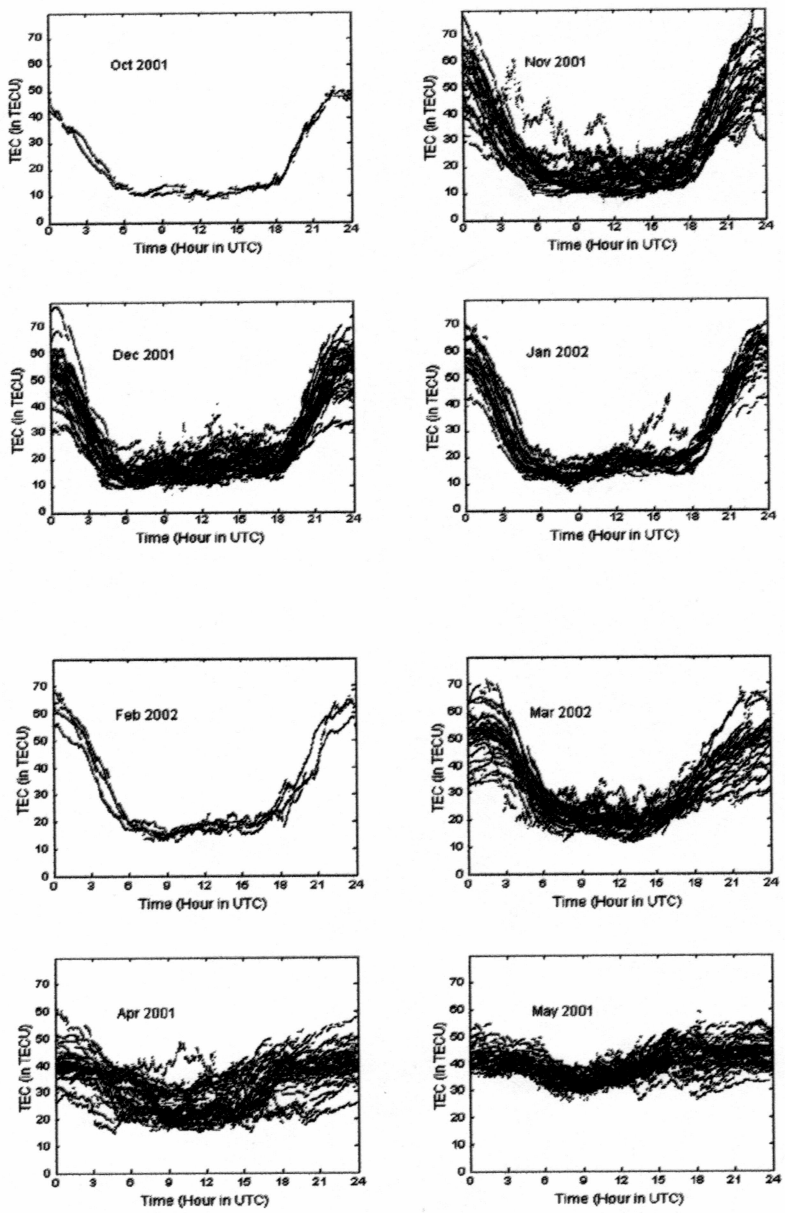

Figure 4.8 Daily TEC plotted to the month.

The coefficients value can be determined according to TEC data having been collected. The daily TEC according to month is plotted in Figure 4.8.

The data used to get those coefficients should be reliable and accurate. The monthly TEC average data shown in Figure 4.9 can be used to calculate them. Due to time constraints the RAM model results are not presented in this thesis.

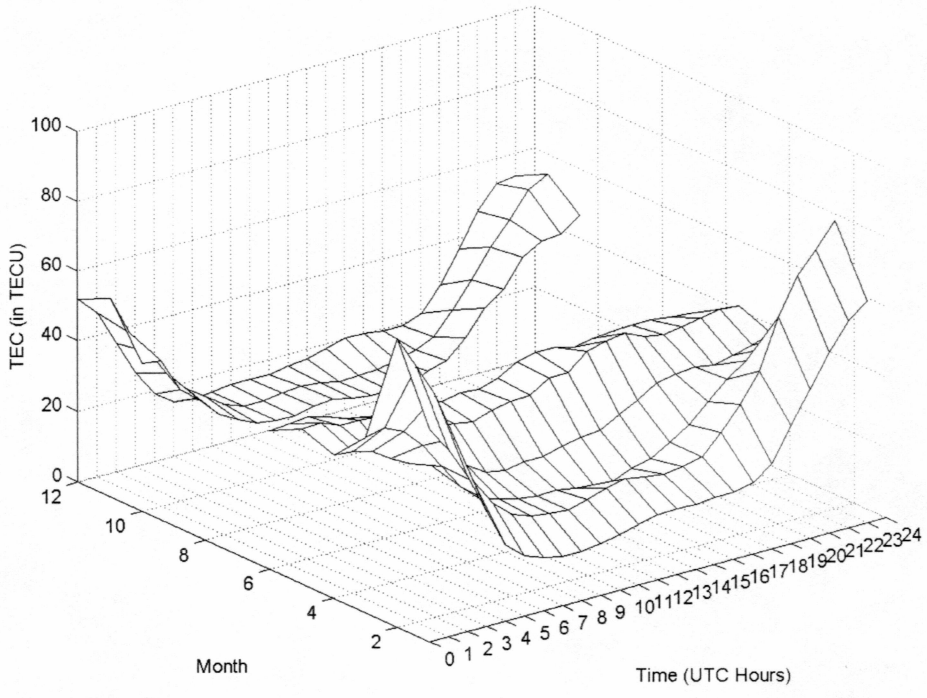

Figure 4.9 3-D plot of monthly average daily TEC. Lines shown on the ground is the TEC contour map with respect to daily hour time and month time.

3. TEC Contour Map with Respect to Time

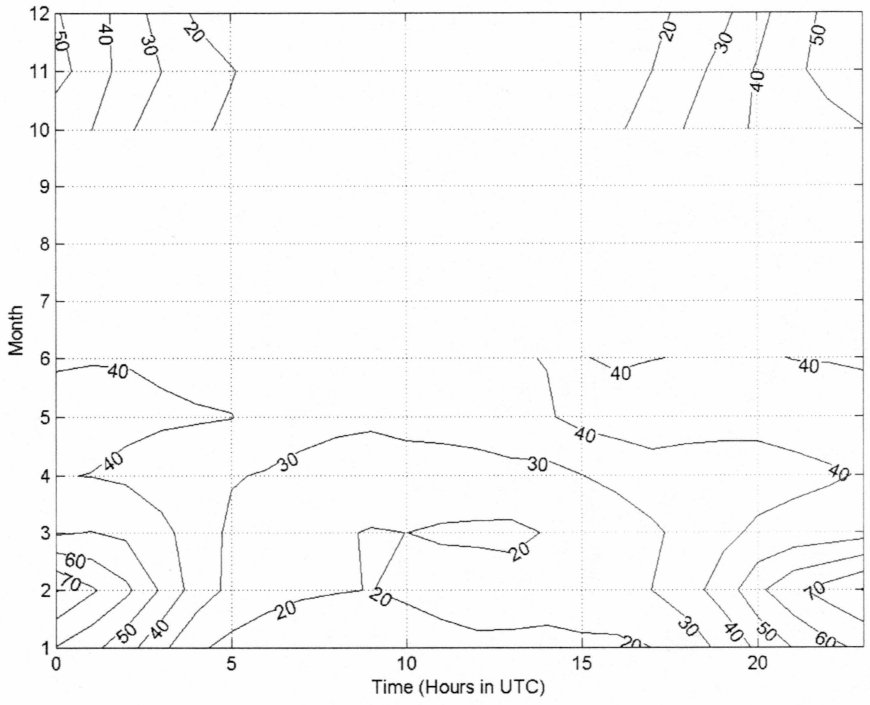

Figure 4.10 TEC contour map with respect to daily hour time and month time.

Shown in Figure 4.10 is the daily average TEC contour map with respect to month. The months 10 to 12 are from the year 2001, and months 1, 2, 3, 4, 5, and 6 are from the year 2002. Months 7, 8 and 9 have not been collected. It is seen that daily TEC variation in winter times is much bigger than summer times.

D. TEC Predication Models

Though the RAM model can give a simplified quick overview of TEC, it is a model that does not consider the physical processes involved in the ionosphere variation. There are two generally acknowledged ionosphere models: International Reference Ionosphere (IRI model) and Parameterized Ionospheric Model (PIM). Both can be used to predict the TEC variation based on time, sunspot number, geomagnetic activity, and geometric input. These models are complex in principle, involving all kinds of mathematical simulation functions, and have been verified by historic ionosphere data, especially by those in the northern hemisphere. Both models will be applied to the TEC data collected, and to the prediction based on the model program. In the end, another non-pre knowledge prediction method using a neural network will be presented and tested by the data. Finally, the comparison results will be discussed.

1. TEC Prediction Using IRI Model

The IRI ionosphere model is an international standard for the specification of ionospheric densities and temperatures, which was developed and recommended by the International Union of Radio Science (URSI) and the Committee on Space Research (COSPAR).

The latest version of IRI is IRI 2000 [7]. IRI is an empirical model based on previous data records. It includes solar indices, such as sunspot number (often the 12-month running mean of sunspot number will be used in IRI), and solar radio flux at 10.7 cm wavelength, which can be obtained from ground observation sites. Thus the forecast of ionospheric parameters will be dependent on the forecast of these solar

indices. Also the IRI model is being updated with measured parameters, such as the TEC deduced from GPS. It is the user's responsibility to specify the input parameters such as location and times to do these updates. Then from the updates, the corresponding IRI index is adjusted until the predicted data matches the measured data. Thus the IRI model provides a way to map the ionosphere globally.

N. Papitashvili at the National Space Science Center provides a java program to implement the IRI model. The program can predict daily TEC variation by the input of latitude, longitude, height, time, month and year. For Fairbanks's GPS site, the input parameters are set as below.

Longitude: $64^{\circ}51'28''$ N

Latitude: $212^{\circ}11'1''$

Height: from 50 km to 20, 200 km (but actually in the IRI model the maximum height for 1 km integration of electron density is 3000 km). For the other solar and geomagnetic input parameters, the program will find them in the database by locating the time.

From execution of the java program at the IRI on-line model site, the corresponding prediction of TEC at Fairbanks is presented in Figure 4.11. It should be noted that the on-line IRI model is based on IRI 95.

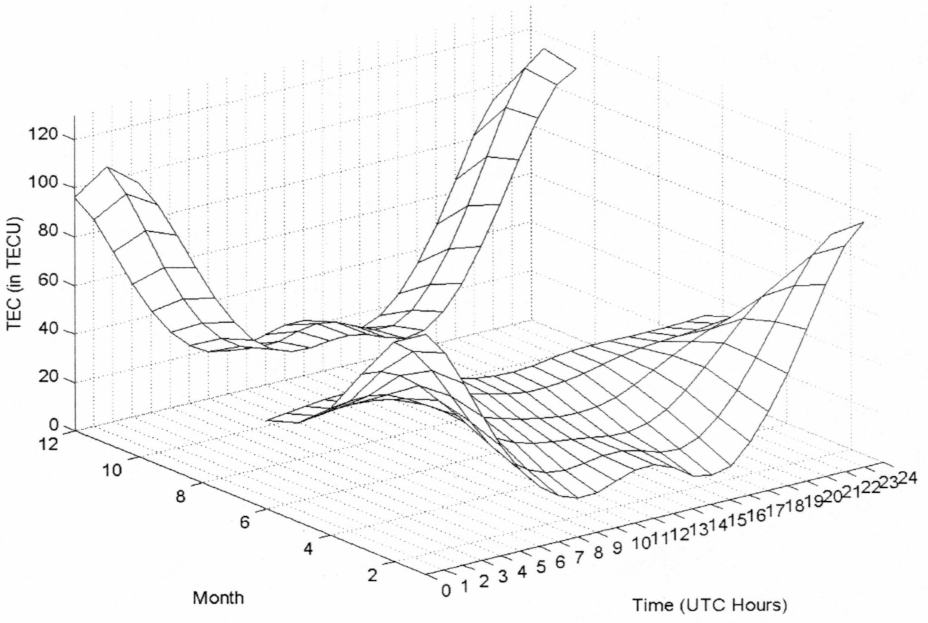

Figure 4.11 3-D plot of monthly average daily TEC from IRI predictions. Lines shown on the ground is the TEC contour map with respect to daily hour time and month time.

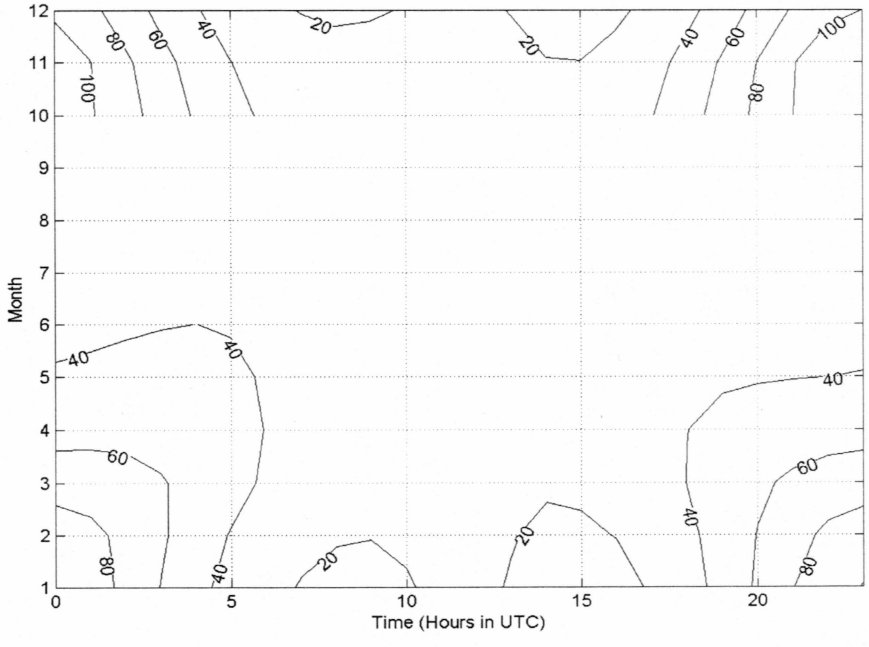

Figure 4.12 IRI predicted TEC contour map with respect to daily hour time and month time.

Also plotted in Figure 4.12 is the TEC contour map according to the prediction by the IRI model. It is found that the maximum TEC is overestimated at solar maximum (2001), especially for the month of October, November, and December of 2001. For the months within 2002 (solar activity dropping down from maximum, but still belonging to the solar maximum), the IRI-estimated TEC matched the measured TEC very well.

Comparing the IRI prediction in Figure 4.11 with the real TEC measurement by the GISTM system in Figure 4.9, we find that for winter times the IRI prediction overestimated the maximum daily TEC value. That can be seen from the bar figure of the percentage error of the IRI prediction Figure 4.13.

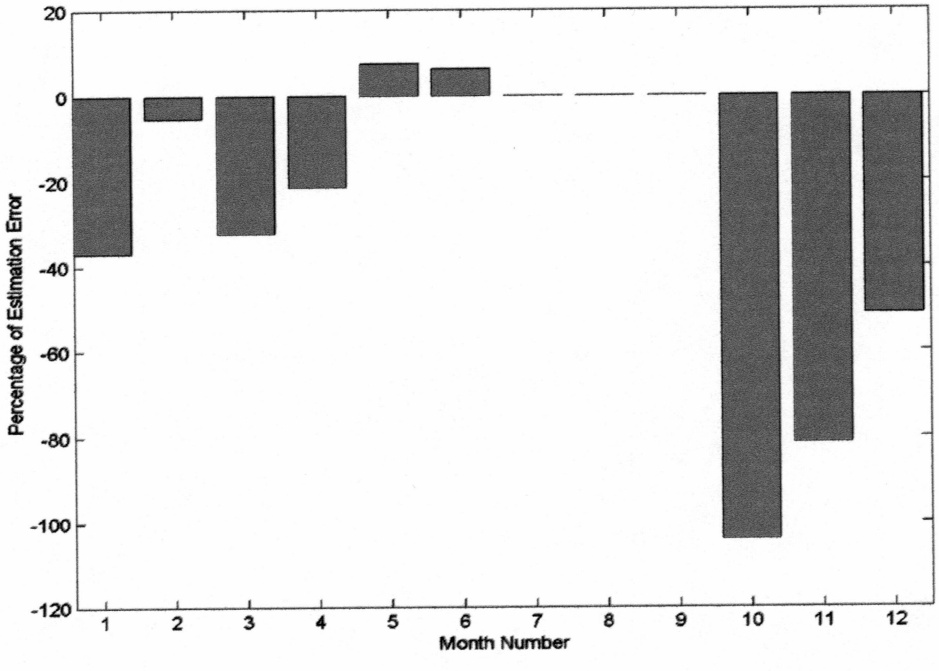

Figure 4.13 Error bar showing the percentage error of IRI on estimating monthly average TEC. Note: the error is calculated by real TEC minus the TEC estimated by IRI.

The IRI model allows predictions to a maximum height of 3000 km, while the GPS deduced TEC is actually above this limit including the protonspheric electron content between 2000 km and 20,200 km. So from the above analysis, the IRI model overestimates the TEC at the solar maximum period.

2. TEC Estimation Using PIM Model

The Parameterized Ionospheric Model (PIM) is a theoretical ionosphere model intending to do real time ionosphere specification for the Air Force Air Weather Service for use at the Air Force Space Forecast Center. The PIM model was initially a computationally efficient model to aid development of a global Parameterized Real-time Ionospheric Specification Model. It is based on four physics-based numerical ionospheric models covering the E and F layers for all latitudes, longitudes, and local times. The four physical ionospheric models are: (1) the Low-Latitude F Layer Model (LOWLAT), (2) the Mid-Latitude F Layer Model (MIDLAT), (3) the High Latitude Model, i.e., Time Dependent Ionospheric Model (TDIM), and (4) an E region Local Chemistry Code. Thus, the PIM model is based on physics simulation of the ion drift and electric fields, rather than an empirical model like the IRI [17].

Currently the PIM model of the high latitude is still under verification by historical data. For high latitude, the PIM model uses the generation of orthogonal polynomials to approximate the ion density by specifying the polynomial coefficients by history database [17]. The database consists of ion density profiles for a set of geophysical conditions on a discrete grid of latitudes and longitudes for a 24-hour period of UT. After specifying the geophysical conditions ("theoretical climatology"),

the program code designed with FORTRAN will extract this data from the database for particular geophysical conditions and spatial coordinates.

The current version of PIM is PIM 1.7, which can be downloaded from the Computational Physics Incorporated website. PIM considers the following geophysical parameters: Year, Day of the year, Universal Time, Solar activity indices F10.7 and Sunspot Number, Magnetic activity index Kp, and Orientation of the y and z components of the interplanetary magnetic field (IMF By and IMF Bz), Latitude and Longitude, and Altitude. The output of PIM is a number of ionospheric parameters like the E and F2 regions' critical frequencies, the corresponding altitudes, and TEC on the grid of rectangular latitude/longitude [5]. So PIM is a global model convenient for the geophysical output on a single Universal Time point, rather than sequential time points in one UT day.

R. E. Daniell told me by email that, "Because PIM was derived from PRISM (Parameterized Real-time Ionospheric Specification Model), which was intended to provide a global ionospheric specification at a given instant of time, PIM can only produce output for one specific UT." In order to predict ionospheric parameters for a period of time, PIM needs to be executed repeatedly for the desired UT sequence of times. R. E. Daniell said that the ability to predict over a period of time would be an important improvement of a future new version of PIM if he had the financial support to maintain the code.

Thus it is a tedious job for prediction of a sequence time. So only one day's TEC prediction above Fairbanks is presented in Figure 4.17 along with the prediction

from IRI and the neural network for comparison. It shows that PIM underestimates the TEC compared to the actual measurement. It can be explained that the PIM model can only produce the electron density profiles up to the altitude of 1600 km [17]. The electron content above this altitude limit cannot be obtained from the PIM model.

The estimation of TEC at Figure 4.17 by PIM uses the input elements as shown in Table 4.1.

Table 4.1 Input parameters for PIM model on day 173 of year 2002. They are coming from the solar weather forecast service by Space Environment Center.

Year	Day	Latitude (Degree)	Longitude (Degree)	F10.7 ($10^{22}Wm^{-2}Hz^{-1}$)	Geomagnetic Activity Index Kp
2002	173	64.85	212.18	142	7

3. TEC Short Term Forecast Using Neural Network

The estimation of TEC from both the IRI and PIM models is based on the input of the solar activity indices, and the magnetic activity index. So the prediction quality from IRI and PIM is dependent on the prediction of these non-ionospheric parameters. Now we examine a third method of TEC prediction, by input of only the previous TEC data. It is assumed that no better indicator of ionospheric behavior than the ionosphere itself unless there is a big change to the ionosphere, like a solar storm.

Allon W. V. Poole had proposed a method of using a neural network to predict f_0F2 over a short time by input of previous ionosphere data only [1]. From the correlation of f_0F2 and TEC, it is possible to do a similar short time forecast of TEC for several hours ahead, even 25 hours ahead.

A back propagation neural network was designed with the input of the hour number, day number, 5 hours previous TEC data, and 30-day average hourly TEC data, with an output of the 5 hours ahead TEC prediction (also 1 to 4 hours ahead, and 25 hours ahead), as shown in Figure 4.14. This kind of design includes the diurnal variation and seasonal variation of the ionosphere. The hour number HR is converted into two quadrature components according to the equations below [1],

$$HRS = \sin(\frac{2\pi \cdot HR}{24})$$

$$HRC = \cos(\frac{2\pi \cdot HR}{24}).$$

The day number DN (counted from the beginning of a certain year) is also similarly converted to two quadrature components as below [1],

$$DNS = \sin(\frac{2\pi \cdot DN}{365})$$

$$DNC = \cos(\frac{2\pi \cdot DN}{365}) .$$

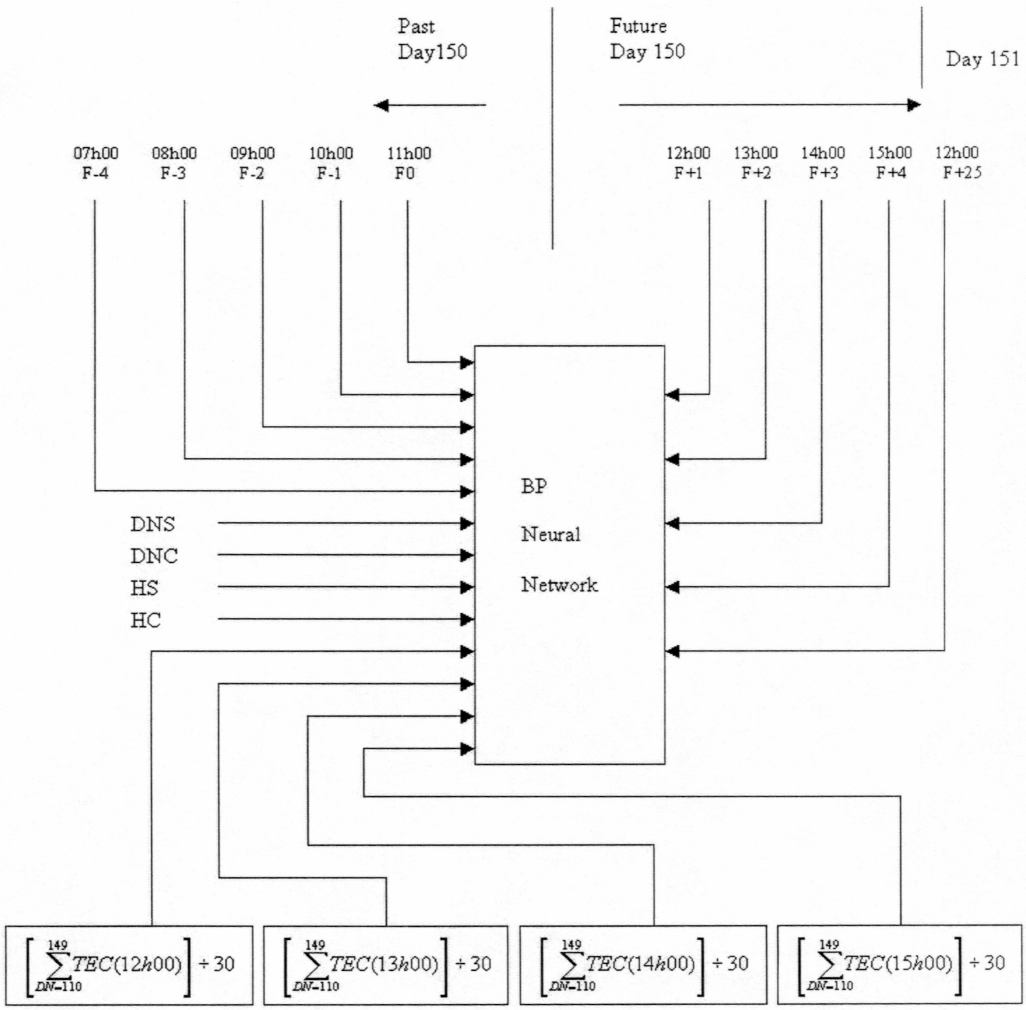

Figure 4.14 Illustrated diagram of the BP neural network design for the TEC short time forecast. The most recently collected TEC data in this example is 11h00 (F0). This Figure is re-plotted from Figure 11 of reference 1.

The input elements include the 5 hours previous TEC data, 30-day average hourly TEC of the desired the estimation hours, and the quadrature components of day number and hour number as shown in Figure 4.14. This kind of design of the input elements considers both the long-term ionospheric behavior by long-term average input and the short time variation by 5 hours previous TEC data inputs. The network is trained by the history data. When the rms of the training error falls to a certain threshold, the training stops. The desired data is set as the inputs, and the TEC estimation of 4 hours ahead, and 25 hours ahead, is obtained from the neural network outputs. The estimation is compared to actual measurements. Figure 4.15 shows a detailed illustration of the training data arrangement. For the program code of the data arrangement and neural network, please refer to Appendix B. 3.

Because of the general consensus that a neural network with more than one hidden layer could not achieve much better performance, the BP neural network implemented as shown in Figure 4.15 is a single layer neural network. It is a fully connected feed forward single layer neural network. The transfer functions for the hidden layer and output layer are hyperbolic tangent sigmoid functions and linear transfer functions respectively.

As to the design of the hidden layer of the BP neural network, the number of the neurons could not be too large, which will cause long training time and memory consumption (less effective), or too small, which will make the network sensitive and unstable (unstable here means the training error can not converge) to the training data. After testing, the number of neurons of the hidden layer was chosen to be 45. The learning rate is automatically set by MatLab functions.

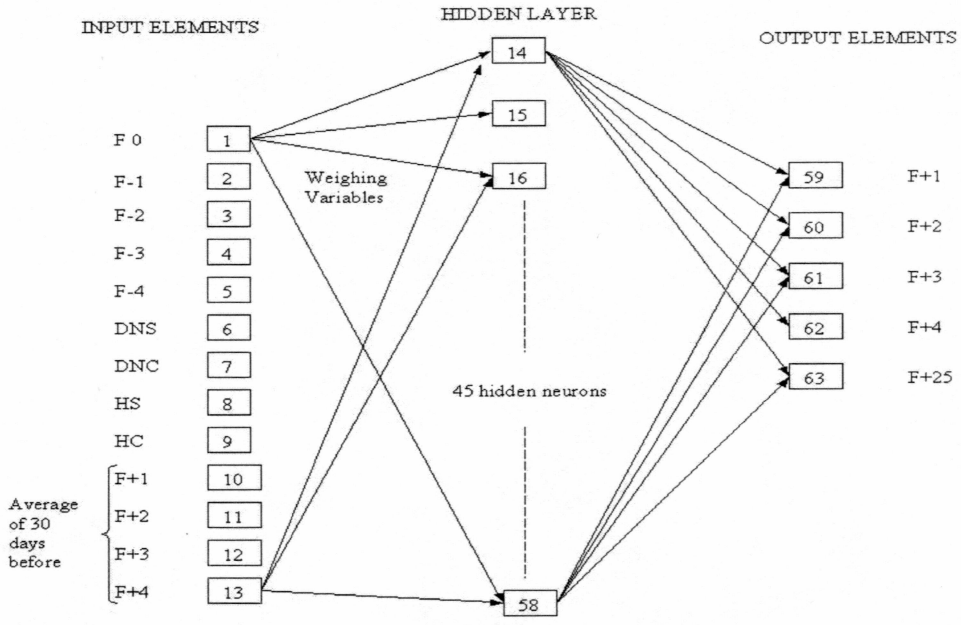

Figure 4.15 The BP neural network internal structure implemented by MatLab neural network toolbox.

The data sets for network training should be near the time of the desired estimation. Also the training data should be continuous without zero measurement gaps. Otherwise it will generate a training matrix with a singularity, which is hard for the neuron network to learn. The first step in manipulating data is to delete the daily data having zero measurements. Then the edited data is applied to train the network. To test this estimation idea, consecutive daily TEC data (averaged to hourly points) from May 1 to June 23 of 2002 were chosen to illustrate this short time estimation. Figure 4.16 shows the TEC estimation results for 1 hour, 2 hours, 3 hours, 4 hours and 25 hours ahead respectively. Each set of training data is trained with 30 epochs. From testing, the rms error between the actual output data set and the target data set is seen to converge. The root mean square (rms) errors between previous TEC data based neural network output prediction and actual TEC data measurement are listed in Table 4.2.

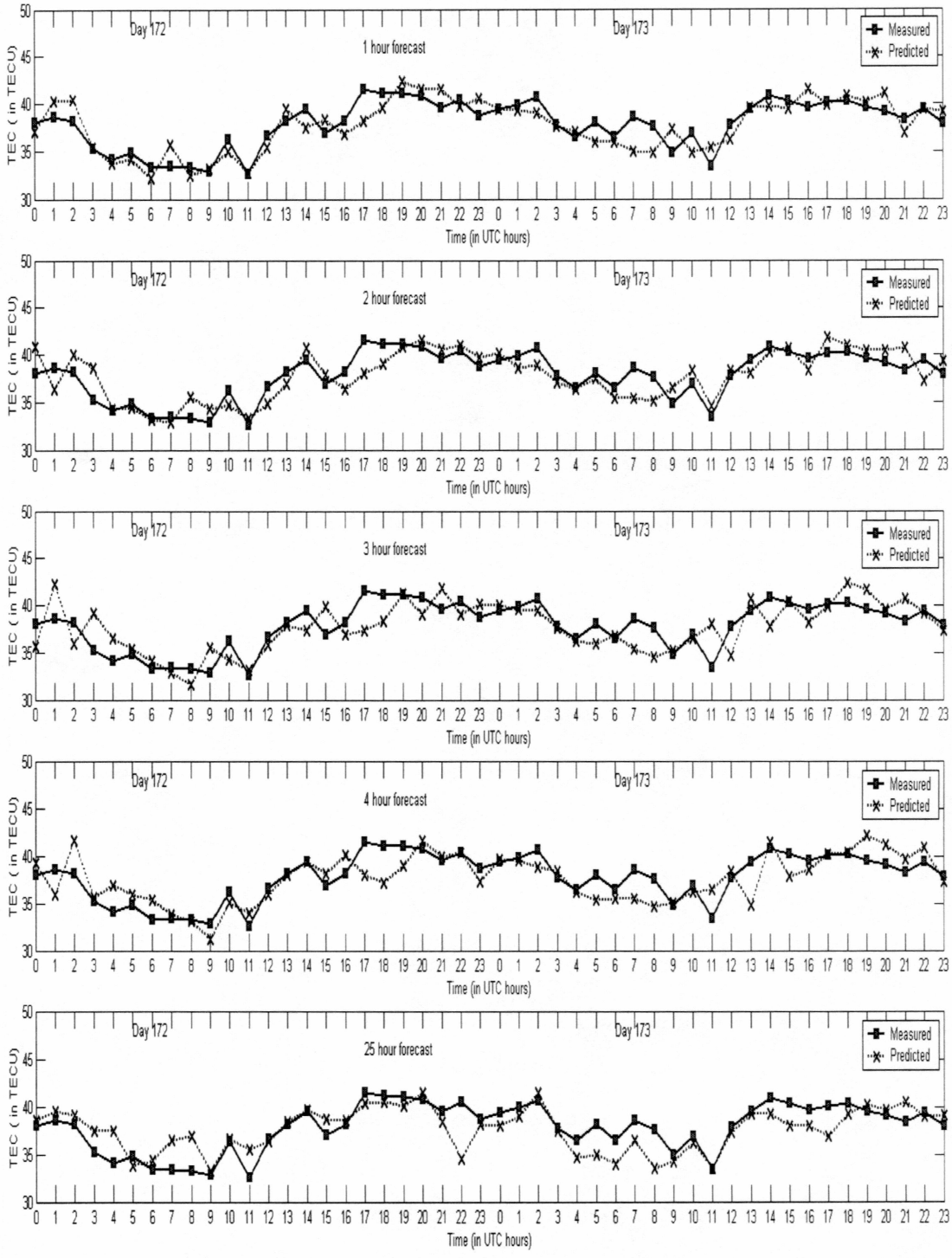

Figure 4.16 Short time estimation output of hourly TEC by 1 hour, 2 hour, 3 hour, 4 hour and 25 hour ahead on day of 172 (June 21) and 173 (June 22) of 2002 with the training data set from May 1 to June 23, 2002.

Table 4.2 Comparison of the rms error between TEC network prediction and actual TEC measurement for five outputs of neural networks as shown in Figure 4.15.

Network Output Elements	**Average rms Error (in TECU) for Prediction Data on day 172 and day 173**
F+1	1.5165
F+2	1.5840
F+3	2.0384
F+4	1.8542
F+25	1.8713

It is seen that the rms error of 1 hour ahead estimation is the smallest. It is understandable that the nearer the time ahead, the more accurate the prediction. However, for 4 hours and 25 hours ahead, the rms errors are less than 3 hours ahead. That might be due to the selection of the training data. The training data might not be perfectly continuous after deleting some zero days. Also the training data set is not large enough to cover all geophysical conditions. Improvement may be done by adding more training data from long time measurements. But the limitation in data collection time is constrained by the available research funding.

The idea of using a neural network to forecast short time TEC variation performs very well which can be seen from Figure 4.17. The rms error is less than 2 TEC units (less than 5 percent).

Compared to IRI and PIM prediction methods, the TEC forecast from a neural network does not depend on the other non-ionospheric information. What it concerns is only the previous TEC data. So it is easier to implement in real time environments than the other two.

4. TEC Prediction Model Verification Results

So far, three kinds of TEC prediction methods have been proposed and tested by real field data measurements. For a direct image of these methods' performance, the three kinds of TEC prediction on one day are plotted in Figure 4.17.

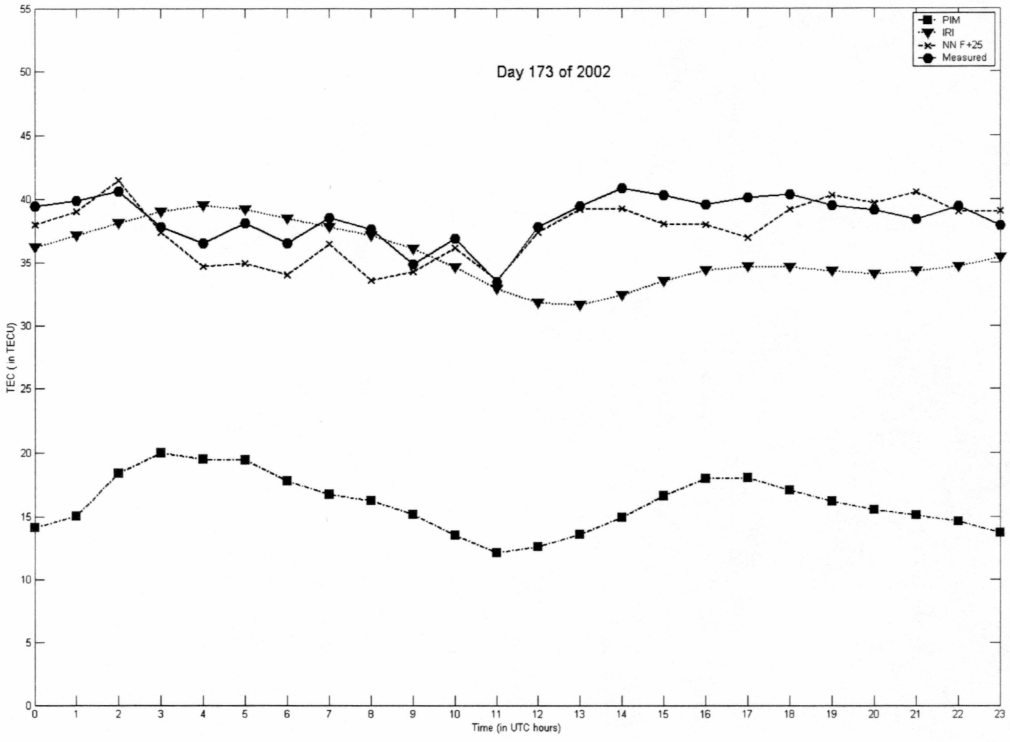

Figure 4.17 Comparisons of TEC predictions from IRI, PIM and neural networks on day 173 of year 2002 (June 22, 2002). Note that the TEC prediction from neural networks is the output of 25 hours ahead.

Table 4.3 List of the rms error between TEC measurement and TEC estimation from PIM, IRI, and BP neural networks 25 hours ahead in Figure 4.16.

Estimation Methods	**Average rms Error (in TECU) for TEC hourly estimation on day 172 and day 173**
PIM	22.6953
IRI	4.3350
Neural Network F+25	1.7620

From Figure 4.17 and Table 4.2, it is shown that the estimation from PIM is not as good as the other two. As mentioned above, the PIM model is a good ionosphere model for geophysical locations for prediction on the longitude and latitude coordinate, which can give a good estimation based on the physical locations rather than the time sequence. So for estimation on the time axis, the other two methods can give much better results.

Another explanation of discrepancy between the model prediction and TEC measurement could be the measurement algorithm adopted. The transformation of slant TEC to vertical TEC might not be accurate.

It is apparent that a neural network is good at the short time estimation of TEC rather than the long time estimation. For long time estimation of TEC, the IRI model should be used. For the global map of TEC on the geo-coordinate, the PIM or IRI model is recommended.

E. Relationship between TEC and Ionosphere Scintillations

The remote sensing of the ionosphere through measuring TEC by GPS gives us a way to probe into the solar and magnetic effects causing variation of the ionosphere, which involves a knowledge of geophysics and chemistry. But the electrical engineer's main concerns are the corresponding effects to electrical systems like satellite to ground communication systems, long wave radio broadcasts, etc., in which the signal amplitude fluctuations and signal scintillations are dominant factors. For modern communication systems with high performance circuits, signal amplitude fluctuations within the link budget margin are not a big problem compared to phase scintillations. The phase scintillation near GPS signal frequencies comes mainly from ionospheric irregularities. In this part, both amplitude and phase scintillation effects by the ionosphere will be thoroughly studied by examining real scintillation data from GPS measurements.

1. Analysis of Amplitude Scintillation Index Data

The rate of amplitude scintillation at high latitude positions is relatively slow, which can be indicated by spectral analysis of the S4 index at one single satellite track, for PRN #8 on March 25, 2002, as shown in Figure 4.18. It is shown that the amplitude scintillation is moderate to low and not as serious as that occurring in the equatorial areas. Also after examining the S4 data, it is found that the data collection antenna has a strong impact on amplitude scintillation. The choke ring antenna has a better performance on depressing the amplitude scintillation caused by multipath than the pinwheel antenna, and thus better represents atmospheric caused scintillation.

Also much of the amplitude scintillation is coming from the lower atmosphere (troposphere) in conditions of such as rain, or snow etc., rather than the ionosphere.

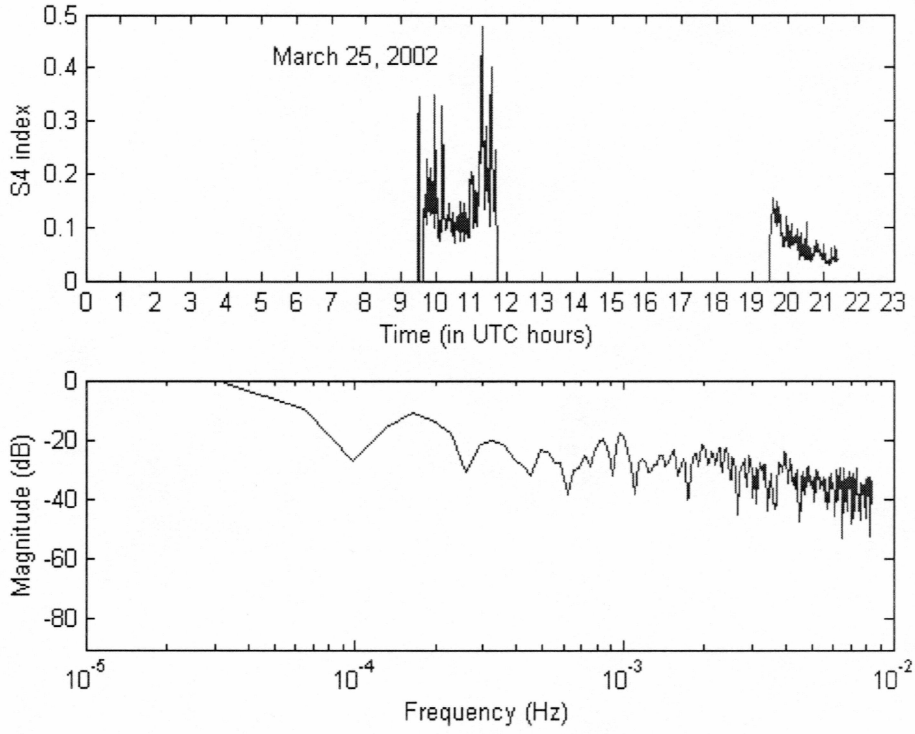

Figure 4.18 Spectrum of S4 index by PRN #8 on day of March 25, 2002.

Much of the amplitude scintillation comes from multipath reflections. It is demonstrated that the antenna has a great impact on amplitude scintillation by calculation of percentage of exceedance time of S4 on four consecutive days with two different antennas installed as shown in Figure 4.19. After the pinwheel antenna was replaced with the choke ring antenna, that has better performance on depressing the multipath reflection, the amplitude scintillation was much smaller than before, which is indicated by smaller exceedance percentage as in Figure 4.19.

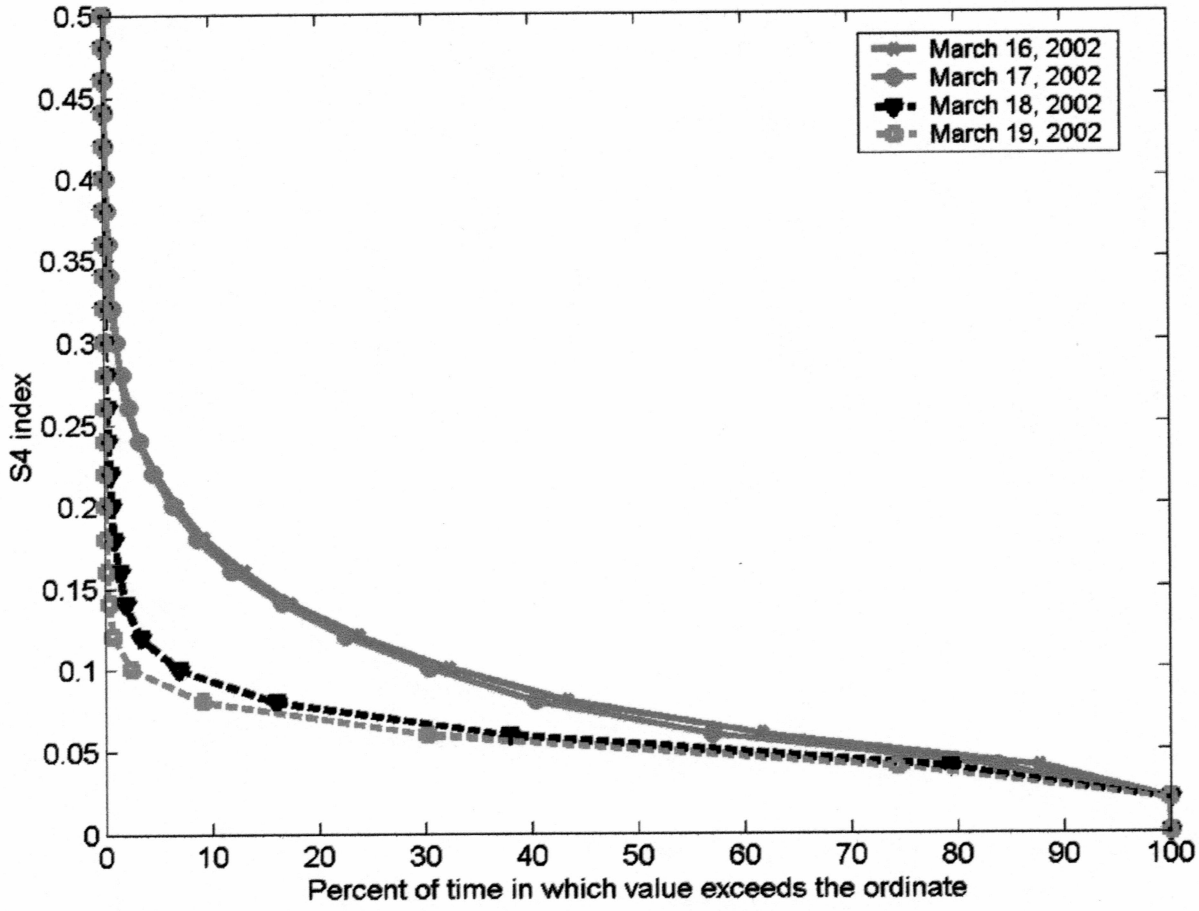

Figure 4.19 Comparison of impact on S4 index by changing different antennas. Note: the pinwheel antenna was used on days March 16-17, 2002; choke ring antenna was used on days March 18-19, 2002.

On the other hand, in order to distinguish the sources of amplitude scintillation, the S4 index and sigma of 60-second code carrier standard deviation can be plotted together as shown in Figure 3 of reference 8. A high value of the standard deviation of code to carrier divergence reflects signal variations due to multipath as mentioned above, while a low value of the standard deviation of code to carrier divergence indicates atmospheric induced scintillation. That is because the divergence of code to carrier variations with respect to multipath is much faster than those with respect to the ionosphere.

2. TEC's Impact to Phase Scintillation and Relationship between Amplitude Scintillation and Phase Scintillation

The major effect to communication systems caused by the ionosphere is phase scintillation, which is indicated by the parameter of phase sigma collected by the GISTM. The measurement of 60-second phase sigma will not be accurate unless the lock time of the receiver to carrier phase on L1 is longer than 240 seconds [10]. It is shown that the data collection of phase sigma in Figure 4.20 satisfies this requirement.

The irregularities in ionospheric structure or rapid change of TEC can bring serious phase scintillations. It is found that the rate of change of TEC has positive correlation to phase scintillation, which can be shown in Figure 4.20. Also the multipath activity as mentioned above, which is indicated by the standard deviation of code to carrier divergence, also causes phase scintillation. That means the phase scintillation comes from both multipath and rapid TEC changes.

On the other hand, there is no strong linkage between phase scintillation and amplitude scintillation, which can be illustrated by Figure 4.21, showing both the S4 index and 60-second phase sigma for all PRNs within one day.

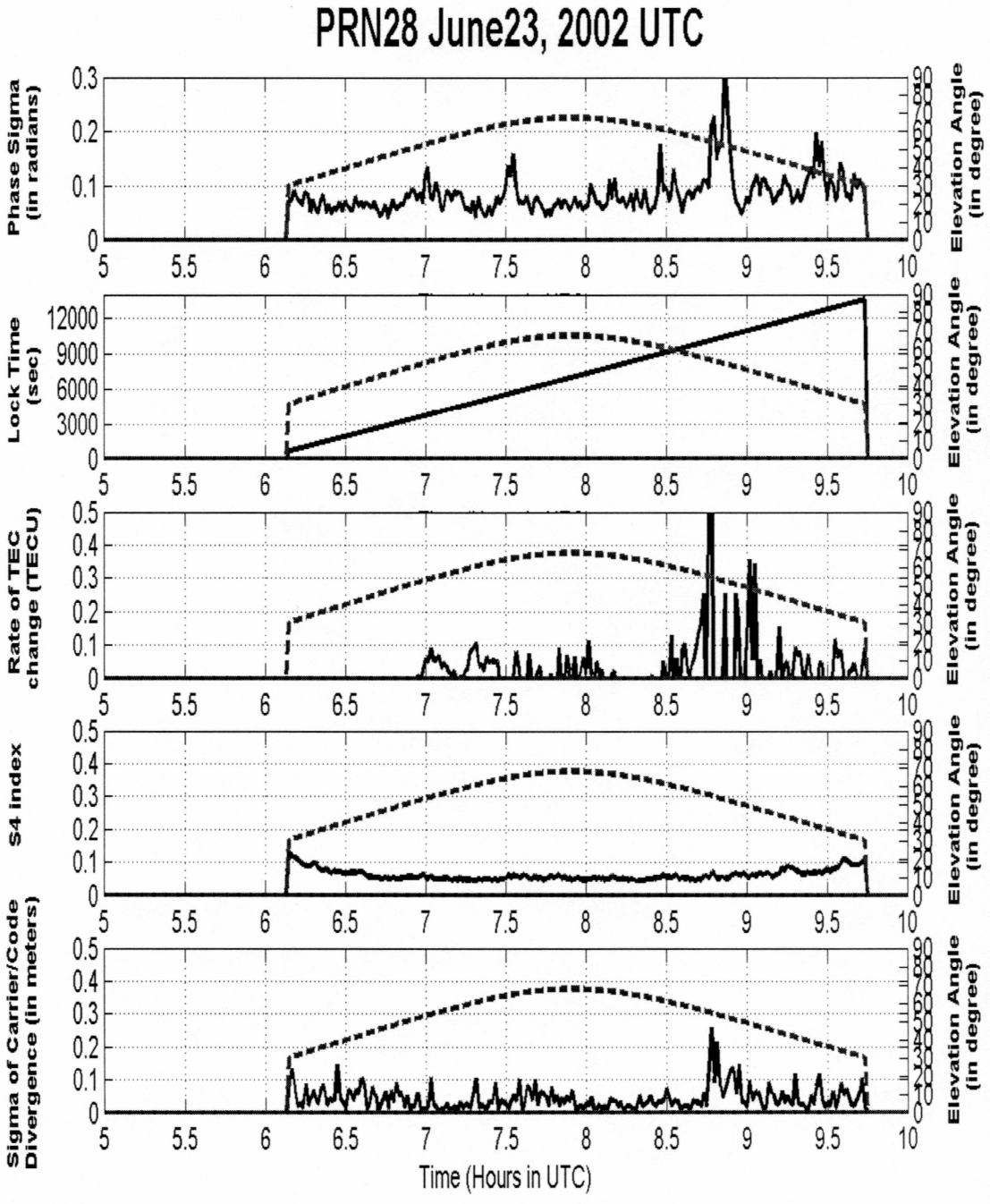

Figure 4.20 Illustration of impact to phase scintillation from rate of TEC change. The data were from PRN # 28 of June 23, 2002. Note: the TEC change was recorded every 15 seconds, then averaged in one minute, then being plotted vs. time in hours as shown in the figure.

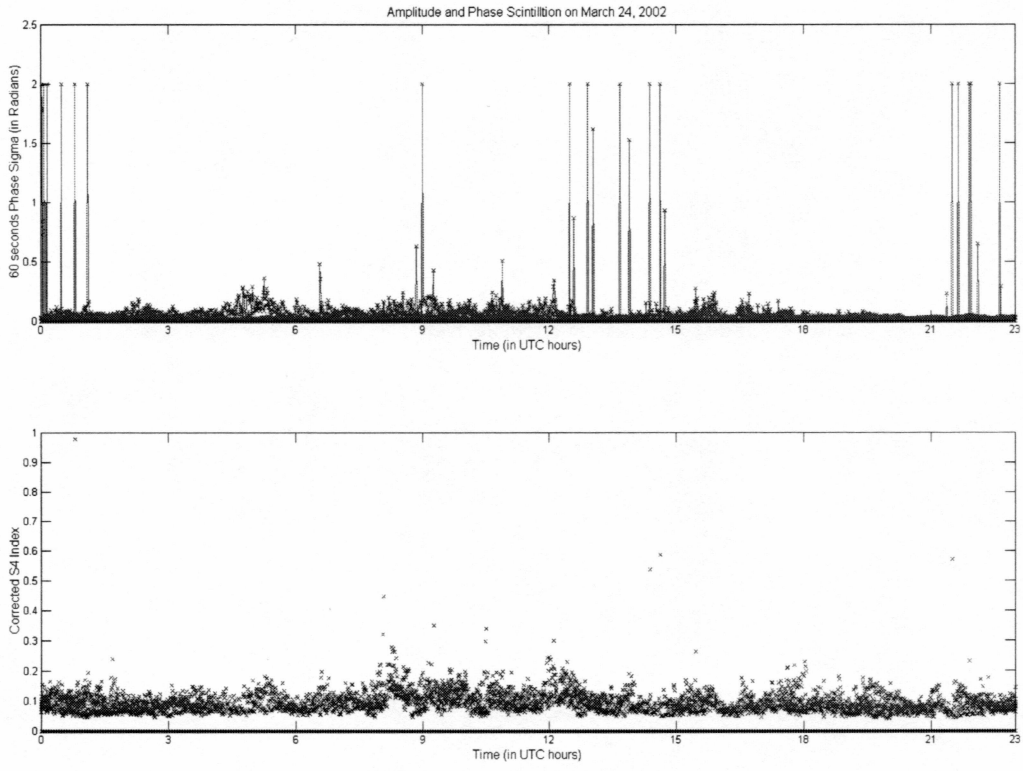

Figure 4.21 Amplitude and phase scintillation illustration for day of March 24, 2002 of all PRNs available. Note: for sigma of 60-second phase scintillation index larger than 2 radians, the corresponding value had been set to be 2 radians. The reason is that sigma of phase scintillation measurement greater than 2 radians might be machine measuring errors.

Overall, for most of the time both amplitude and phase scintillations are moderate for high latitude areas. Peak daily phase scintillation usually occurs between 5 am to 8 am and between 9 pm and 12 pm. This is just a rule of thumb for dates around equinox. For particular dates in winter or summer, it may vary with sunset time.

F. TEC Daily Contour Map Around Fairbanks

After the study of TEC prediction models comparison and the impact to scintillation effects due to TEC variation, it is useful to get the contour map of the TEC and its real time display, which can give an intuitive image of how the ionosphere varies in a short time.

The display of a TEC contour map along the satellite track is shown by available data. As discussed in previous sections, the TEC measurements by GPS is restricted to specific tracks of GPS satellites. So the contour map obtained is also constricted to certain areas due to the available satellite tracks. Figure 4.22 displays the TEC measurement in one single day on physical coordinates. There is no constraint on the elevation angles. So the TEC measurement on the north of Fairbanks is also included by the plot.

It should be noted that this kind of plot has many disadvantages as the data are coming from all the different time points within one day. It has an internal assumption that the TEC does not change a lot within one single day. But in actually this is not the case. However, if we choose the TEC data within a short time, such as 15 minutes or 1 hour, or even 3 hours (contour map for 3 hours is shown in Figure 4.23), the number of data points is not sufficient enough to get the contour map across the whole sky. Instead blank data points due to no GPS satellite tracks cover most of the sky as shown in Figure 4.24. If we want to separate the adjacent data points along a satellite track within a short time, the dimension of the matrix for contour plot should be very large.

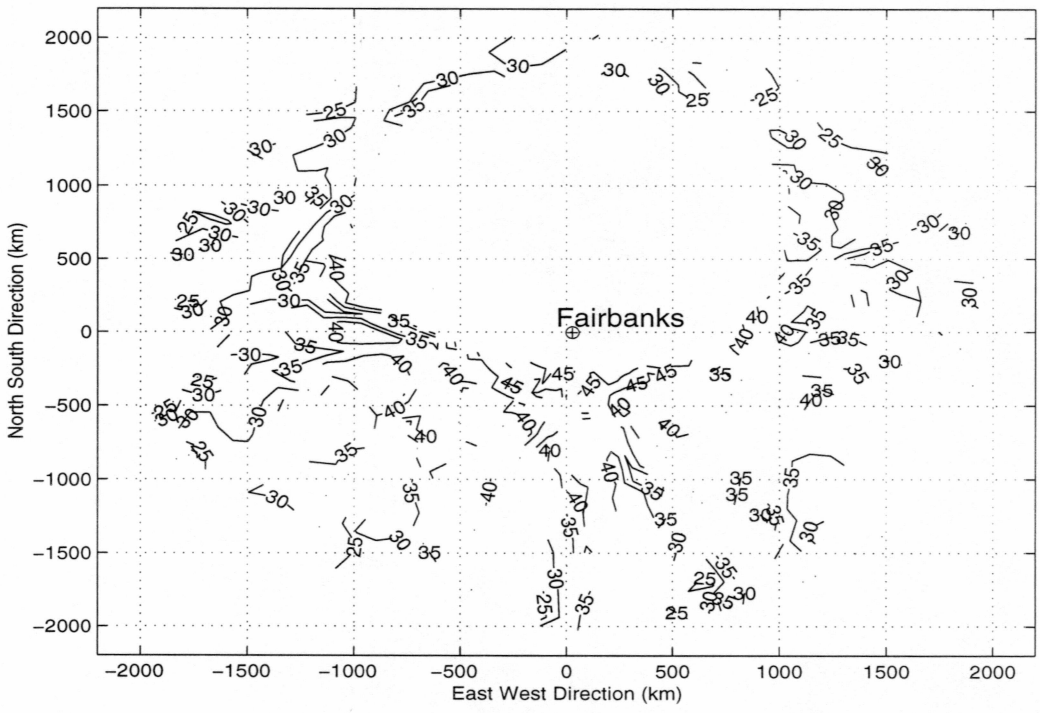

Figure 4.22 TEC contour map along satellite tracks measured on June 22, 2002. The number along the line is TEC value in TECU unit.

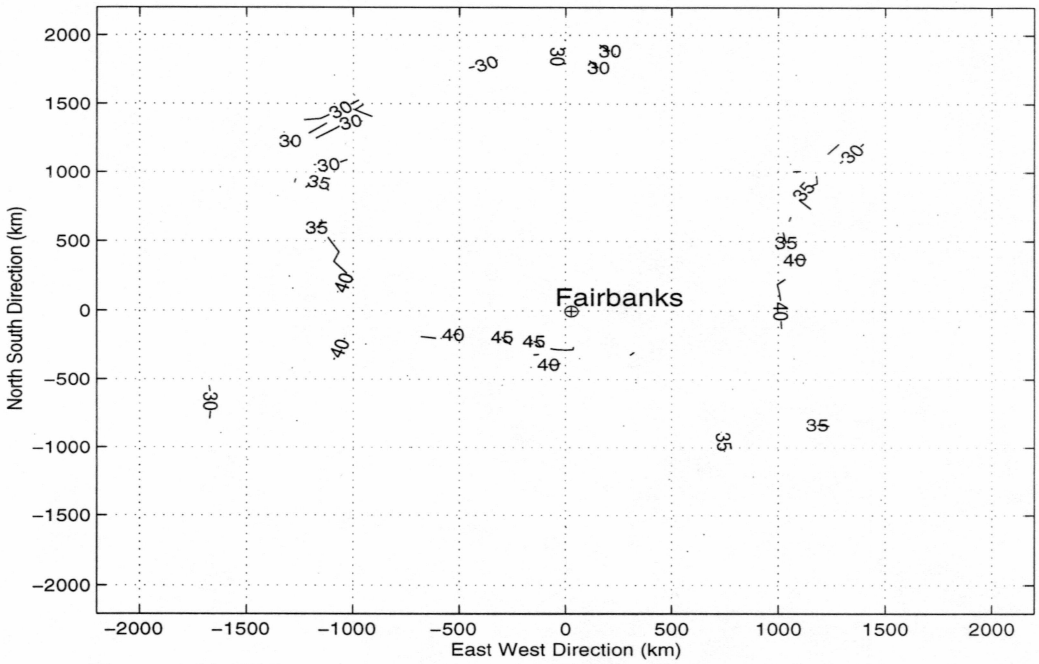

Figure 4.23 TEC contour map along satellite track measured from 0 am to 3 am on June 22, 2002. The number along the line is TEC value in TECU unit.

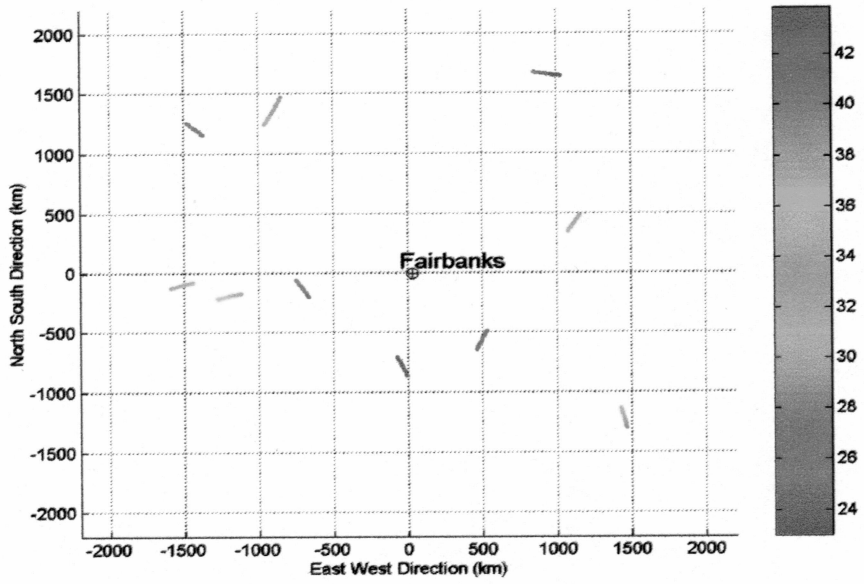

Figure 4.24 Satellite moving tracks within 15 minutes from 17:12 to 17:22 (UT) on day of June 22, 2002

Thus the data points are very sparse in the contour matrix, which makes it difficult to obtain the contour map within a short time scale. The daily contour map of TEC is a compromise process between size of the data matrix and available TEC data size. The distances in km along different directions are transferred from the elevation angles and azimuth angles of data points based on the effective ionospheric penetrating point height (for the transformation of elevation angle to physical distance, please refer to Appendix A). Also Figure 4.25 shows the surface map of daily TEC measurement and Figure 4.26 shows the short time TEC surface map within 3 hours. There is an apparent round blank area due to the area not covered by GPS satellite tracks. From Figure 4.22 and Figure 4.25, we can see the TEC overhead has the highest value, while as the TEC in the lower elevation angles has a relative small TEC value. This is because the measurements in the most distant areas (corresponding to the lower elevation angles) have much bigger measurement errors

as mentioned in previous sections. However, it provides a direct image of what the ionosphere looks like within one day, though only in part of the sky for northern high latitude areas.

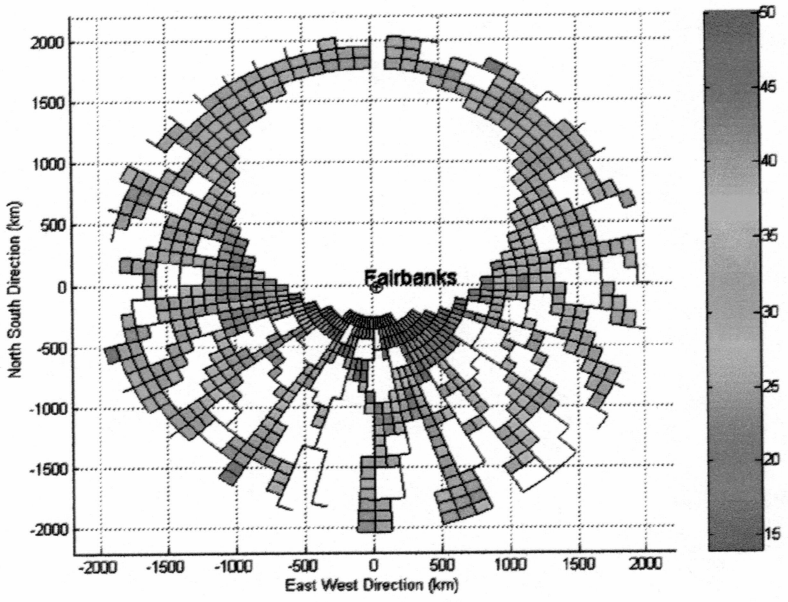

Figure 4.25 Surface map of TEC measurement on day of June 22, 2002. The number along the color bar is the TEC value in TECU unit.

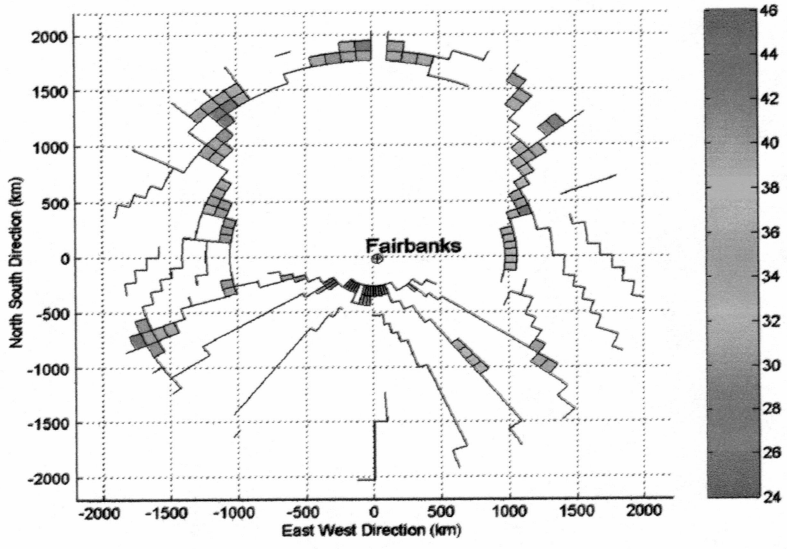

Figure 4.26 Surface map of TEC measurement from 0 am to 3 am on June 22, 2002. The number along the color bar is TEC value in TECU unit.

G. Real Time TEC Display along the Satellite Tracks

At last the real time TEC display in a 3-D coordinate is presented with available data as shown in Figure 4.27. As discussed in part F, the number of TEC data points within a short time is not large enough to get the TEC contour map. So the real time TEC display is illustrated by both the TEC insertion to a rectangular matrix (Figure 4.27 (a)) and physical coordinate (Figure 4.27 (b)) respectively.

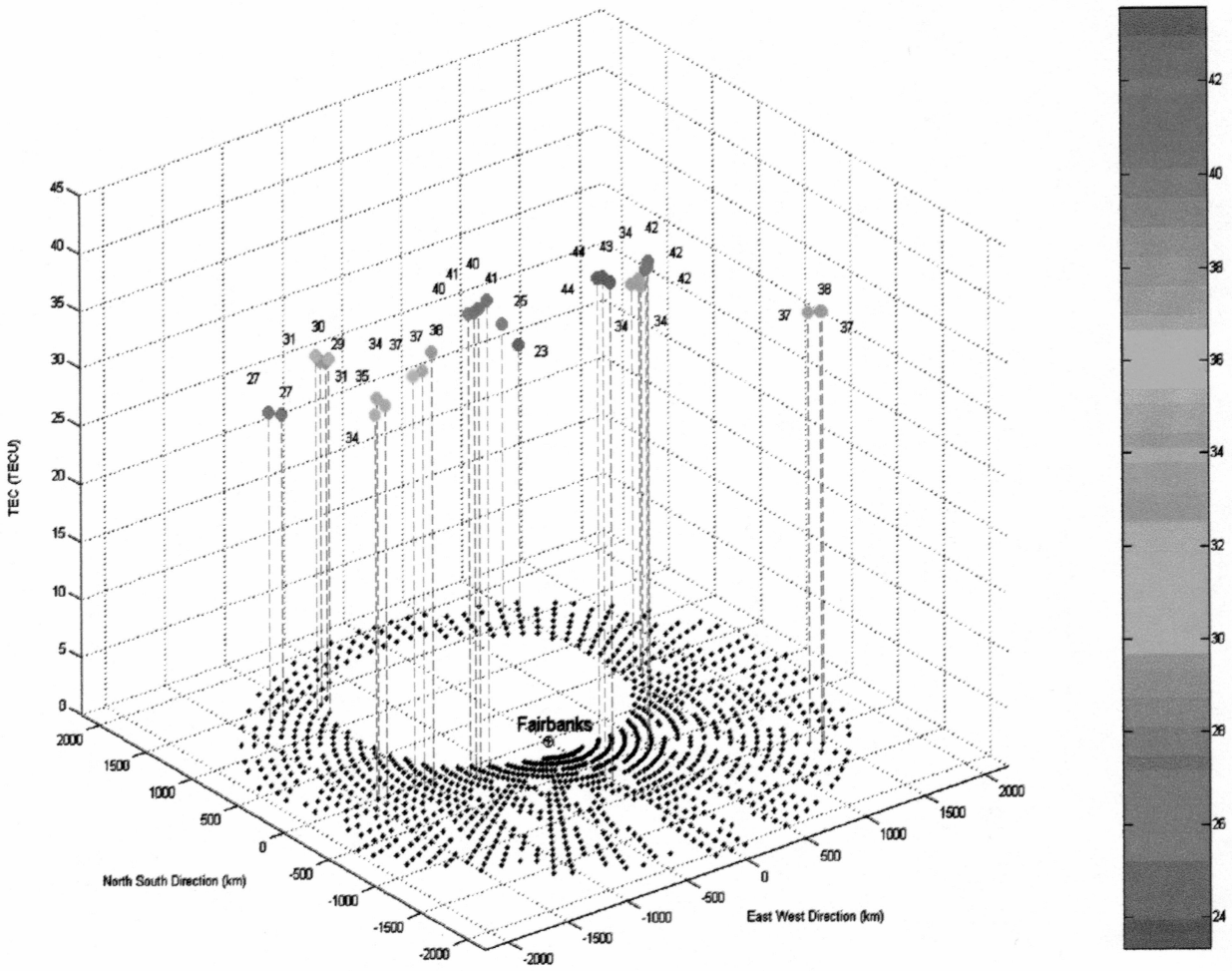

(a)

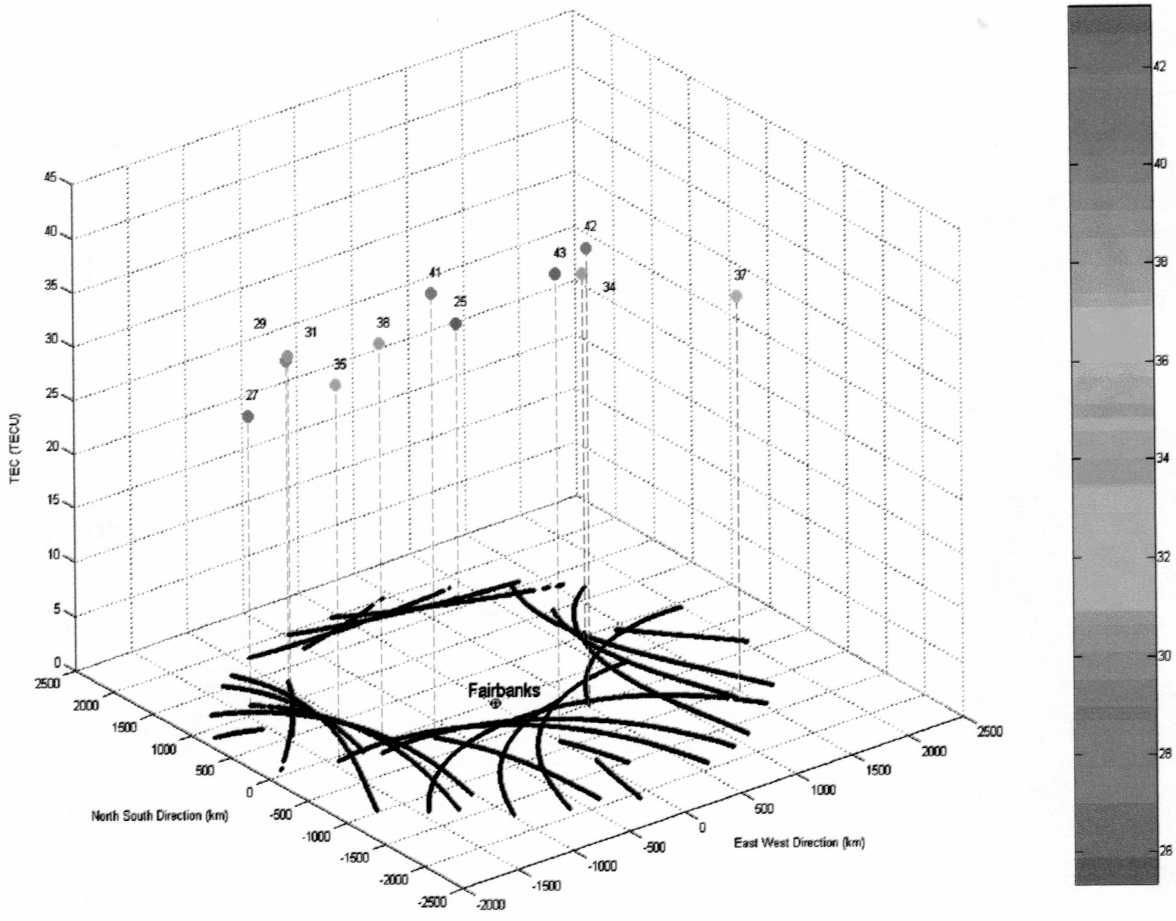

(b)

Figure 4.27 TEC real time 3-D display.

(a) TEC real time 3-D display at from 17:12 to 17:22 (UT) on day of June 22, 2002 with other TEC data points on that day shown underneath. Note: this display is based on the data insertion into a big rectangular matrix. So it may occur that several adjacent data points may be inserted into one data position in the matrix.

(b) TEC real time 3-D display at 17:12 (UT) on day of June 22, 2002 with satellite tracks before that time point shown underneath.

H. Real Time Display of Amplitude Scintillation Index and Phase Scintillation Index

Also the amplitude index S4 and 60-second phase sigma can be plotted in 3-D, which is shown as in Figure 4.28 (a) and (b) respectively.

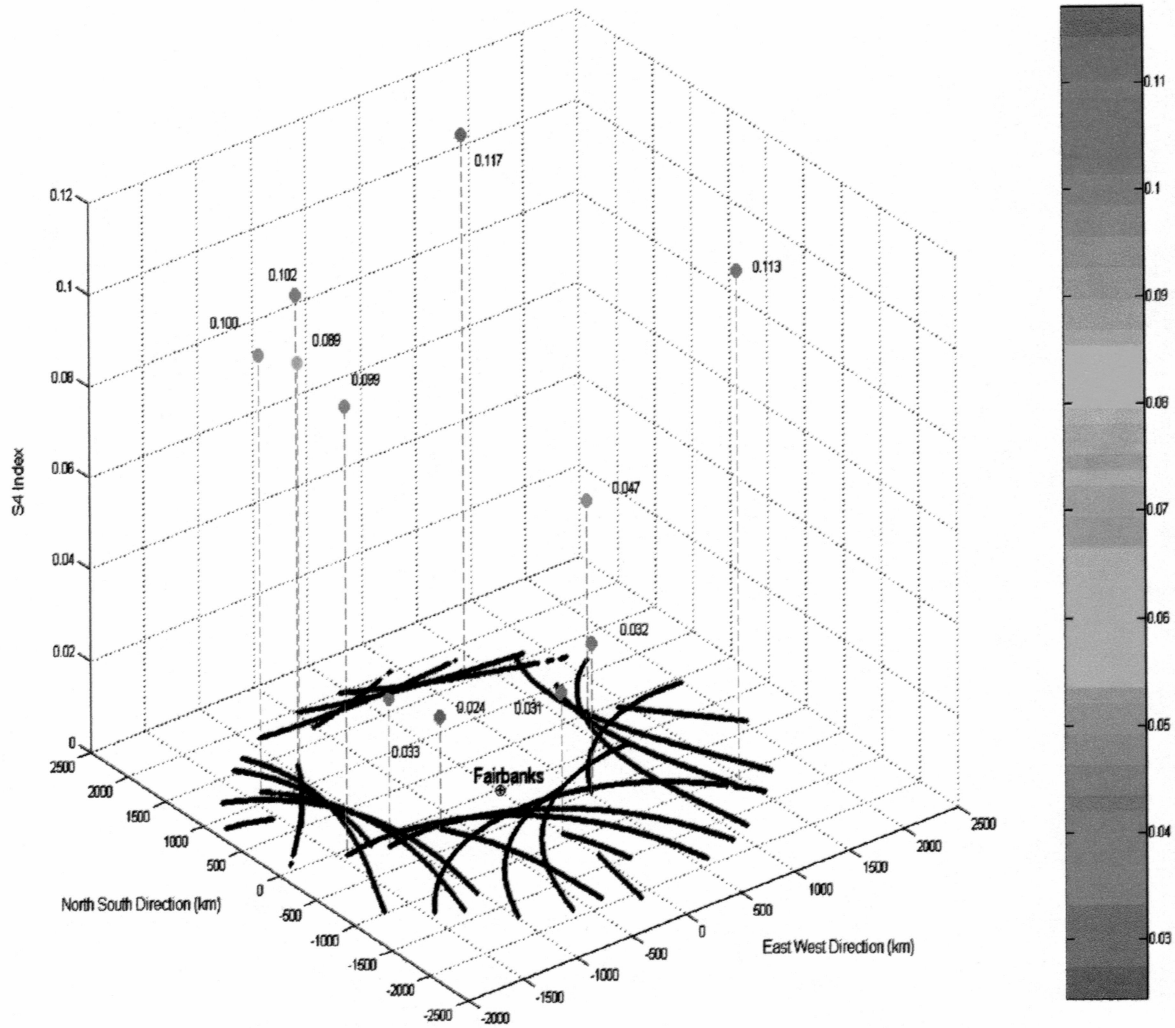

(a)

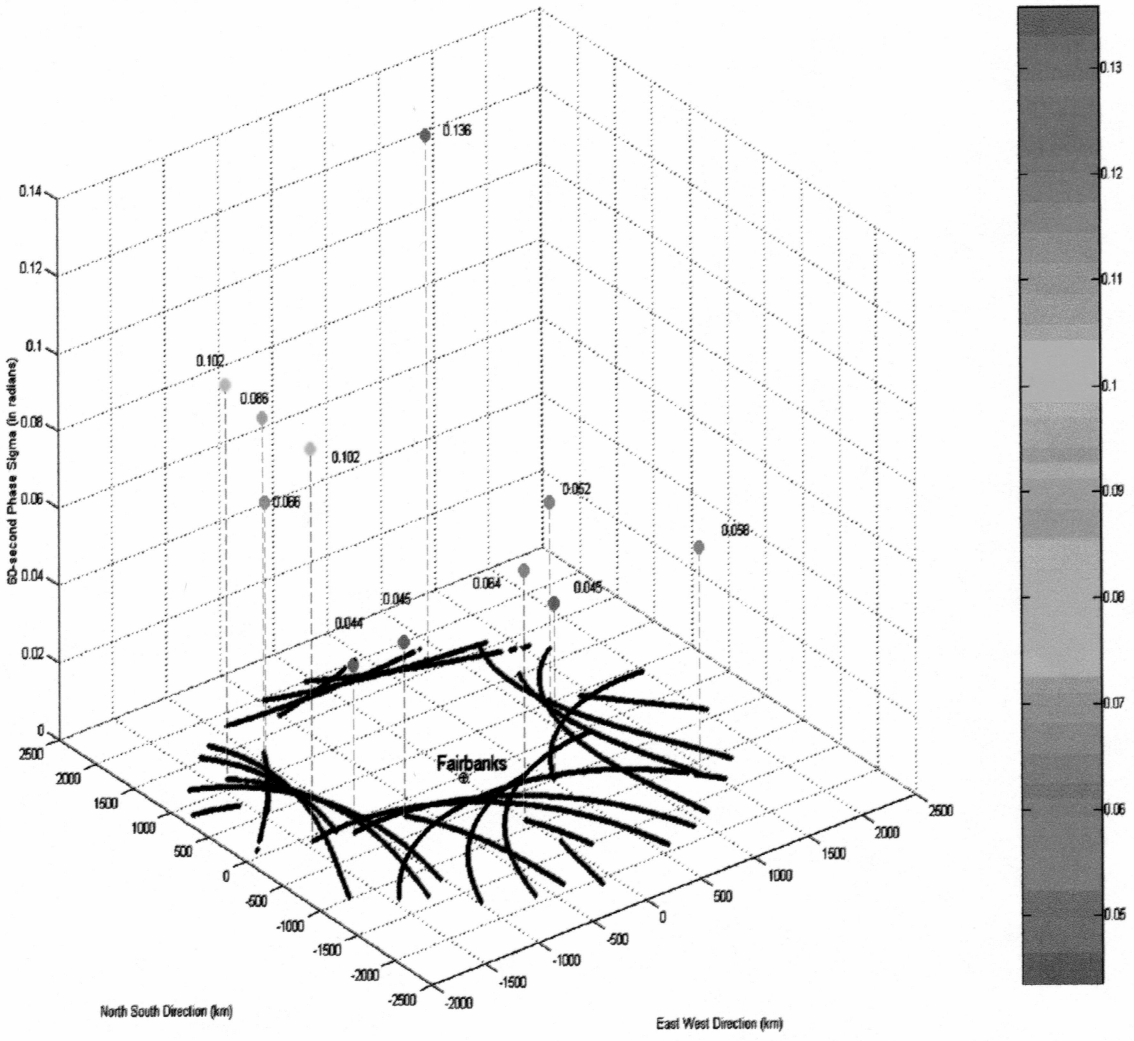

(b)

Figure 4.28 Real time 3-D display of scintillation index at 17:12 (UT) on day of June 22, 2002 with satellite tracks before that time point shown underneath.
(a) S4 index. (b) 60-second phase sigma.

V. Summary and Conclusions

This thesis provides a way of using a GPS receiver to monitor ionospheric scintillations and total electron content of the ionosphere. Also it gives a simple method to monitor ionospheric effects to communication systems. The data were analyzed by different ionospheric models to offer a model verification study for a northern high latitude area.

The research proceeded in three steps. The first step was the setup of the GPS Ionospheric Scintillation and TEC Monitor and raw data collections. In this procedure, an important issue was the naming of the files to distinguish the data from different days. Two different antennas were installed in sequence to test the antenna's impact on data quality. The "**slog**" program automatically recorded the data within one day to one distinct file by set the logging time to exactly one Universal Time day. A link budget from GPS satellites to a ground receiver was also roughly calculated using available data.

The next step was the data parsing work. C++ programs were written to parse the binary raw data into a text data format for easy offline data analysis in a MatLab environment. The thresholds of ionosphere data can be easily set in this step. The data were arranged in time sequence according to the data file names. The raw data were backed up both on the dual hard disks and CD copies. Also the data were published on the Internet for public research.

The last step is the most important step of the research: data analysis of both total electron content and scintillation effects from the ionosphere. First the TEC from typical days were displayed along with the critical frequency of the F2 layer. The critical F2 frequency calculated from TEC shows a good match to that measured by HAARP. So it provides a way to deduce the critical frequency of the F2 layer by TEC measurement. Next, TEC data were modeled by IRI (an empirical model), and PIM (a physical model) ionosphere models. Both models were used to predict the long time and short time TEC variations. Due to the internal structure of the models, the prediction can only be performed to certain altitudes. These limits are 2000 km and 1600 km for IRI and PIM respectively. The TEC prediction from the IRI model is overestimated of during times of strong solar activity, and the prediction from the PIM model is underestimated.

Both IRI and PIM need the input of non-ionosphere data. Based on the assumption of using only ionosphere data, another non-priori knowledge idea of using a BP neural network to do short time forecasting is performed and tested with real data collection. Using the input elements of day number and hour number, long time corresponding hourly average TEC and short time TEC before estimation, both the long time and short time TEC variation were considered and learned by the neural network. After being trained by the available training data set, an estimation was performed and compared with results from IRI and PIM. The comparison shows that for short time TEC data forecast, the BP neural network yields the best performance. However, for long time estimation, the IRI model is recommended for northern high

latitude areas; otherwise, for geographical map estimation of different geographical points on a single UT time point, the PIM model is recommended.

The last step of the data analysis is the investigation of the scintillation effects due to the ionosphere. Overall, for most of the time both amplitude and phase scintillations are moderate for high latitude areas. By spectral analysis of the S4 index, the rate of change of amplitude scintillation is seen to be slow. Also the antenna plays an important role of depressing amplitude scintillation due to multipath reflections. Both rapid changing TEC and multipath reflections can cause phase scintillations. However, there is no strong link between amplitude and phase scintillations. That means there are different causes of the two scintillations. For amplitude scintillation, sources are mainly clear sky effects, water vapor or snow. For phase scintillation, ionosphere irregularities is the one of the important sources. At last, the TEC contour map along satellite tracks above Fairbanks within one day is displayed.

From the work done so far, it can be concluded that GPS gives a way to collect ionosphere data globally and time seamlessly. If a GPS receiver network is set up, global real time monitoring of the ionosphere is possible, except at the north and south poles due to GPS satellite tracks. Also the BP neural network can be used to forecast TEC variation in short time scale rapidly and accurately.

Appendix A.

Discussion of Round Circle of GPS Satellite Tracks in Northern High Latitude Areas

Due to the 55 degrees inclination of orbiting tracks by GPS satellites, there is a round blank area that is not covered in the sky in both northern and southern high latitude areas. Typical satellite tracks within one day shown Figure A. 1.

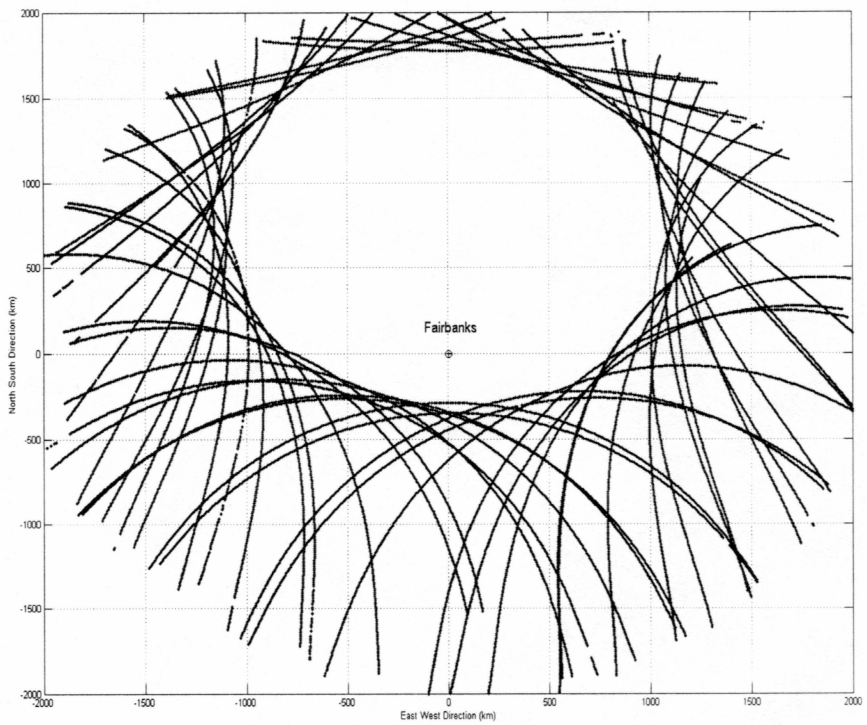

Figure A.1 Satellite tracks within day of June 22, 2002.

It should be noted that the distance displayed in Figure A. 1 is transformed from the satellite elevation angles with 0 degree corresponding to 2200 km. The transformation process is shown as below.

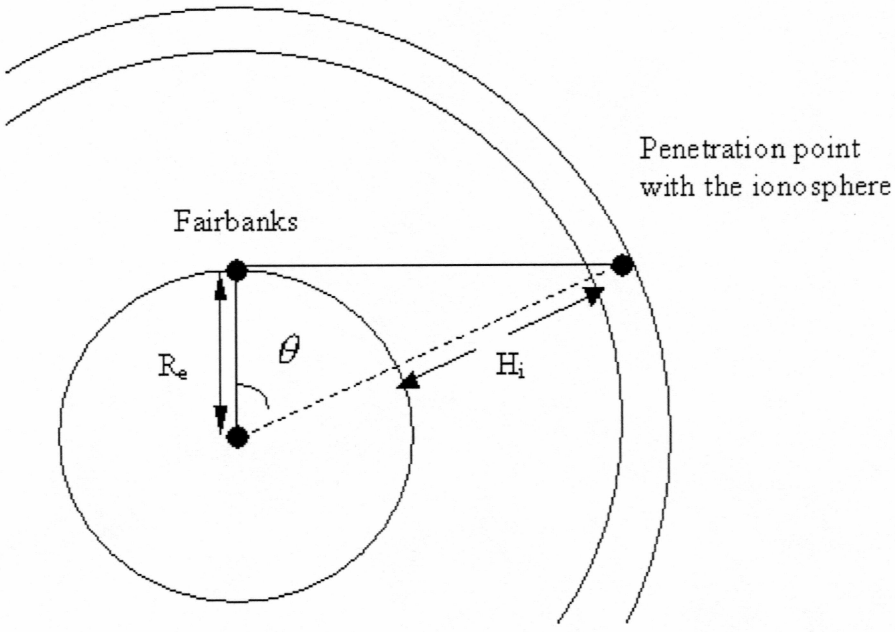

Figure A.2 Distance transformations from elevation angles.

H_i shown in Figure A.2 is the effective ionosphere height. Usually we choose H_i to be 400 km. When satellite elevation angle is zeros, angle θ as shown in Figure A.2, could be calculated as

$$\theta = \cos^{-1}\left(\frac{R_e}{R_e + H_i}\right) = \cos^{-1}\left(\frac{6371}{6371+400}\right) = 19.79^\circ \qquad \text{(A.1)}$$

R_e in equation (A.1) is the radius of the Earth. Thus we can calculate the big arc distance D on the Earth from the zeros degree elevation angle signal penetration point with the Earth to Fairbanks, which is shown in equation (A.2).

$$D = \frac{\theta}{360^\circ} \times 2 \times \pi \times R_e = 2200 \text{ [km]} \qquad \text{(A.2)}$$

Thus the zeros elevation angle corresponds to the physical distance of 2200 km. We can scale this relationship to other elevation angles. This is the principle of distance transformation.

Appendix B. Program Lists

Appendix B lists some of the programs used in the work. Program written in script configuring GISTM system for binary data collection is listed in part B.1. Program written in C++ for parsing the binary data to text format is listed in part B.2. Program written in MatLab for vertical TEC plot is listed in part B.3. At last the program for BP neural network for short time TEC forecast is listed in part B.4.

B.1 Program List for Slog

```
;Initiate communication with the receiver

find com1 57600 scint time
send * "log com1 bestposa ontime 60 \r"

label again

jumpport TimeIsSet COM1 gpsset() == TRUE
pause 1.0
jump again

label TimeIsSet
jump again GPSWEEKSECS() > 604800-10

define double T

let T = 86400-(GPSWEEKSECS()-86400*floor(GPSWEEKSECS()/86400))

find com1 57600 scint time

    ;Log firmware version and request 60-second logs
    send * "log com1 versiona once\r"
    send * "log com1 bestposa ontime 60 \r"
    send * "log com1 ismrb onnew\r"
    send * "log com1 rangeb ontime 60\r"

    pause T+60

loopstart Oneweek
    find com1 57600 scint time

    ;Log firmware version and request 60-second logs
    send * "log com1 versiona once\r"
    send * "log com1 bestposa ontime 60 \r"
    send * "log com1 ismrb onnew\r"
    send * "log com1 rangeb ontime 60\r"

    pause 86400

loopend Oneweek 7
```

B.2 Program List for Binary Data Parsed to Text Data Format

```
/*
 * This source is released into the public domain.
 * Do with it as you will.
 * It MAY not be fit to suit any purpose.
 * Usage: parseismr <PRN_check_bit> <inputfile> > outputfile
 * in which PRN_check_bit means 0 (display only the elevation angle and
azimuth angle)
 * or 1 (display data from every satellite in PRN order).
 */

#include <stdio.h>
#include <stdlib.h>

#define CHANNEL_DATA_SIZE (152)

void
Usage( void)
{
    fprintf(stderr, "Usage: ParseISMR <PRN_check_bit> <inputfile> >
            outputfile\r\n");
    exit(1);
}

void
ParseLog( FILE* fIn, unsigned long ulRequestedPrn )
{
  unsigned long ulChannels;
  unsigned long ulPrn;
  float       fAzimuth;
  float       fElevation;
  bool        check_bit=1;

  fread( &ulChannels, 1, 4, fIn );

  for( unsigned long i=0; i<ulChannels; i++)
       //number of SV obersvations
  {
    fread( &ulPrn, 1, 4, fIn );
    if( ulRequestedPrn == 0 )
    {
      // Just print out PRNs and elevations
      fread( &fAzimuth, 1, 4, fIn );
      fread( &fElevation, 1, 4, fIn );

      printf( ", %d, %0.2f, %0.2f", ulPrn, fAzimuth, fElevation );

      fseek( fIn, CHANNEL_DATA_SIZE-12, SEEK_CUR );
    }
    else if( ulPrn == ulRequestedPrn )
    {
      double dCNo;
      double dS4;
      double dS4Correction;
      double d1SecSigma;
```

```
                double d3SecSigma;
                double d10SecSigma;
                double d30SecSigma;
                double d60SecSigma;
                double dCodeCarrier;
                double dCodeCarrierStdDev;
                float fTEC45;
                float fTECRate45;
                float fTEC30;
                float fTECRate30;
                float fTEC15;
                float fTECRate15;
                float fTEC0;
                float fTECRate0;
                double dLockTime;
                unsigned long ulStatus;
                double dL2LockTime;
                double dL2CNo;

                fread( &fAzimuth, 1, 4, fIn );
                fread( &fElevation, 1, 4, fIn );
                fread( &dCNo, 1, 8, fIn );
                fread( &dS4, 1, 8, fIn );
                fread( &dS4Correction, 1, 8, fIn );

                fread( &d1SecSigma, 1, 8, fIn );
                fread( &d3SecSigma, 1, 8, fIn );
                fread( &d10SecSigma, 1, 8, fIn );
                fread( &d30SecSigma, 1, 8, fIn );
                fread( &d60SecSigma, 1, 8, fIn );

                fread( &dCodeCarrier, 1, 8, fIn );
                fread( &dCodeCarrierStdDev, 1, 8, fIn );

                fread( &fTEC45, 1, 4, fIn );
                fread( &fTECRate45, 1, 4, fIn );
                fread( &fTEC30, 1, 4, fIn );
                fread( &fTECRate30, 1, 4, fIn );
                fread( &fTEC15, 1, 4, fIn );
                fread( &fTECRate15, 1, 4, fIn );
                fread( &fTEC0, 1, 4, fIn );
                fread( &fTECRate0, 1, 4, fIn );

                fread( &dLockTime, 1, 8, fIn );
                fread( &ulStatus, 1, 4, fIn );

                fread( &dL2LockTime, 1, 8, fIn );
                fread( &dL2CNo, 1, 8, fIn );

                /*
                * Set threshold of the data.
                */
                if( (dS4<1) && (fTEC0>0) && (fTEC0<200) && (dLockTime>240))
                                printf( " %d %0.2f %0.2f %f %f %f %f %f %f %f %f %f
%f %f %f %f %f %f %f %f %f %f %f %f\n",
                  ulPrn,
```

```
                fAzimuth,
                fElevation,
                dCNo,
                dS4,
                dS4Correction,
                d1SecSigma,
                d3SecSigma,
                d10SecSigma,
                d30SecSigma,
                d60SecSigma,
                dCodeCarrier,
                dCodeCarrierStdDev,
                fTEC45,
                fTECRate45,
                fTEC30,
                fTECRate30,
                fTEC15,
                fTECRate15,
                fTEC0,
                fTECRate0,
                dLockTime,
                dL2LockTime,
                dL2CNo );
                        else
                                printf(" %d %s\n", ulRequestedPrn, " 0 0 0 0 0 0 0 0 0 0 0 0
0 0 0 0 0 0 0 0 0 0 0 0 0");
                        check_bit=0;

            }
                        else
            {

                        fseek( fIn, CHANNEL_DATA_SIZE-4, SEEK_CUR );
            }

             }

             if( check_bit )
                        printf(" %d %s\n", ulRequestedPrn, " 0 0 0 0 0 0 0 0 0 0 0 0 0 0 0
0 0 0 0 0 0 0 0 0");

        }

        void
        ScanForLogs( FILE* fIn, unsigned long ulPrn )
        {
          while( !feof( fIn ) )
          {
            unsigned char ch = fgetc( fIn );

            if( ch == 0xAA )
            {
              ch = fgetc( fIn );
              if( ch == 0x44 )
              {
                ch = fgetc( fIn );
```

```
        if( ch == 0x12 )
        {
          unsigned char ucHeaderLength = fgetc( fIn );

          unsigned long ulMessageID = fgetc( fIn );
          ulMessageID |= (fgetc( fIn ) << 8);

          if( ulMessageID == 0x112 )
          {
            // fseek( fIn, ucHeaderLength - 6, SEEK_CUR );
            unsigned short usWeek;
            unsigned long  int ulMilliSecs;

            fseek( fIn, 8, SEEK_CUR );
            fread( &usWeek, 1, 2, fIn );
            fread( &ulMilliSecs, 1, 4, fIn );
                                    fseek( fIn, 8, SEEK_CUR );

            printf("%d %ld", usWeek, ulMilliSecs/1000 );
            ParseLog( fIn, ulPrn );

            fseek( fIn, 4, SEEK_CUR );
          }
          else
          {
            fseek( fIn, 2, SEEK_CUR );
            unsigned long ulMessageLength = fgetc( fIn );
            ulMessageLength += (fgetc(fIn) << 8 );
            fseek( fIn, ulMessageLength + ucHeaderLength - 6, SEEK_CUR );
          }
        }
        else
        {
          fseek( fIn, -2, SEEK_CUR );
        }
      }
      else
      {
        fseek( fIn, -1, SEEK_CUR );
      }
    }
  }
}

int
main( int argc, char* argv[] )
{
  unsigned long ulPrn_bit;
  char*         szFileName;

  if( argc == 2 )
  {
    szFileName = argv[1];
  }
  else if( argc == 3 )
  {
```

```
    szFileName = argv[2];
    ulPrn_bit = atol( argv[1] );

  }
  else
  {
    Usage();
  }

  FILE* fIn = fopen( szFileName, "rb");
  if( fIn == NULL )
  {
    fprintf(stderr, "Can't open file: %s\r\n", szFileName );
    Usage();
    exit(1);
  }
  fclose( fIn );



     if(ulPrn_bit)
     {
       for (ulPrn_bit=1; ulPrn_bit<=31;ulPrn_bit++)
                {
                        FILE* fIn = fopen( szFileName, "rb");
                        ScanForLogs( fIn, ulPrn_bit );
                        fclose( fIn);
                }

     }
    else
                ScanForLogs( fIn, ulPrn_bit );

  fclose( fIn );

  return 0;
}
```

B.3 Program List for Vertical TEC Plot

The program listed below is for the vertical TEC calculation of month April 2002. After calculation, the TEC is stored into MatLab *.mat file for later quick processing.

```
clear all

Index=[2:1:25 28:1:30];
tt=size(Index);

C4=zeros(1439, tt(1, 2));

for i=1:1:tt(1, 2)
   STR1='scint_02apr';
   STR2=num2str(Index(i));
   STR3='.txt';
   t=strcat(STR1, STR2, STR3);
   A = load(t);
   D = size(A);
   n = D(1,1)/31;
   S4 = A(:,7);
   TOW = A(:,2);
   TEC = A(:,22);
   Time = rem(TOW, 24*3600)/3600;
   EL=A(:, 5)*pi/180;

   S1=0;
   S2=1;


   Hi = 400;
   Re = 6356.78;
   VTEC=cos(asin(Re*cos(EL)/(Re+Hi))).*TEC;

   PRN=1;
   var=(floor(n*(PRN-1)+S1*n+1)):floor(n*(PRN-1)+S2*n);

   T_Div = zeros(size(var));
   T_Ab = zeros(size(var));

   for PRN = 1:1:31
      z=0;
      for w = (floor(n*(PRN-1)+S1*n+1)):1:floor(n*(PRN-1)+S2*n)
         z=z+1;

         if (VTEC(w) ~= 0)
            T_Div(z) = T_Div(z) + 1;
         end

         T_Ab(z) = VTEC(w) + T_Ab(z);
      end
```

```
    end

    T_Div1=zeros(1439, 1);
    T_Ab1=zeros(1439, 1);

    for f = 1:1:n
        xy=round(rem(TOW(f), 24*3600)/86400*1440);
        if xy==0
            xy=1;
        elseif xy==1440
            xy=1439;
        end
        T_Ab1(xy)= T_Ab(f)+T_Ab1(xy);
    end

    for g = 1:1:n
        xy=round(rem(TOW(g), 24*3600)/86400*1440);
        if xy==0
            xy=1;
        elseif xy==1440
            xy=1439;
        end
        T_Div1(xy)= T_Div(g)+T_Div1(xy);
    end

    for m=1:1:1439
        if (T_Div1(m) == 0)
            T_Div1(m) = 1;
        end
    end

    AVG_TEC=T_Ab1./T_Div1;
    C4(:, i)=AVG_TEC;
end

save('TEC_day', 'C4', '-append')
```

B.4 Program List for BP Neural Network for Short Time TEC Forecast

```
clear all
close all

load('TEC_day.mat')

% Load TEC daily data to C
C=[C5 C6];

[m, n]=size(C);

%Transfer Day number of the Year
DayC5=[1:1:31]+120;
DayC6=[1:1:23]+151;

DayNum0=[DayC5 DayC6];
[b, d]=size(DayNum0);
X=zeros(24, d);


p=0;
Y=X;
DayNum1=zeros(1, d);

for tt=1:1:d
   Mark=1;
   for i=1:1:24

      for c=((i-1)*60+1):1:i*60-1
         X(i, tt)=X(i, tt)+C(c, tt);
      end

      if X(i, tt)==0
        Mark=0;
      end

   end

   if Mark ==1
      p=p+1;
      Y(:, p)=X(:, tt);
      DayNum1(p)=DayNum0(tt);
   end

end

YY=zeros(24, p);
DayNum=zeros(1, p);

for pp=1:1:p
   YY(:, pp)=Y(:, pp);
   DayNum(pp)=DayNum1(pp);
end
```

```
[x, y] = size(YY);

MM=zeros(1, x*y);

for t=1:1:y
   MM((x*(t-1)+1):x*t)=YY(:, t)/59;
end


%ReArrange original data to P and T training arrays

P= zeros(13, x*y-30*24-25+1);
T= zeros(5,  x*y-30*24-25+1);
i = 0;

for z = 30*24:1:x*y-25
   i=i+1;

   P10=0;
   P11=0;
   P12=0;
   P13=0;

   DN=DayNum(ceil(z/24));
   HR=rem(z, 24);

   P(1, i)=MM(z);
   P(2, i)=MM(z-1);
   P(3, i)=MM(z-2);
   P(4, i)=MM(z-3);
   P(5, i)=MM(z-4);
   P(6, i)=sin(2*pi*DN/365);
   P(7, i)=cos(2*pi*DN/365);
   P(8, i)=sin(2*pi*HR/24);
   P(9, i)=cos(2*pi*HR/24);

   for t = (z-30*24):24:(z-24)
      P10=MM(t+1)+P10;
      P11=MM(t+2)+P11;
      P12=MM(t+3)+P12;
      P13=MM(t+4)+P13;
   end

   P(10, i)=P10/30;
   P(11, i)=P11/30;
   P(12, i)=P12/30;
   P(13, i)=P13/30;

   T(1, i)=MM(z+1);
   T(2, i)=MM(z+2);
   T(3, i)=MM(z+3);
   T(4, i)=MM(z+4);
   T(5, i)=MM(z+25);
```

```
end

%Train the network for 72 hours

D = zeros(5, 72);
TR = D;
for r = 1:1:72

   PR=zeros(13, 2);
   PR(:, 1)=-1;
   PR(:, 2)=90;
   net = newff(PR, [45 5],{'tansig' 'purelin'}, 'trainlm', 'learngdm');

   net.trainParam.epochs = 30;
   net.trainParam.goal = 0.2;
   net = train(net, P(:, 1:(i-72+r-25)), T(:, 1:(i-72+r-25)));

% Output the estimation after the training of the network by previous data.

   D(:, r)=sim(net, P(:, (i-72+r)));
   TR(:, r)=T(:, i-72+r);

end

% Save estimation and real TEC to PredictTEC.mat.
save('PredictTEC', 'D', '-append')
save('PredictTEC', 'TR', '-append')
```

Reference:

[1] Allon W. V. Poole and Lee-Anne McKinnell, "On the predictability of foF2 using neural networks", Radio Science, Vol. 35, Number 1, Pages 225-234, January-February, 2000.

[2] A. M. Breed, et al, "Ionospheric total electron content and slab thickness determined in Australia", Radio Science, Vol. 32, Number 4, Pages 1635-1643, July-August 1997.

[3] Assistant Secretary of Defense for Command, Control, Communications, and Intelligence, "Global Positioning System Standard Positioning Service Performance Standard", Department of Defense, October 2001.

[4] Basrur Rama Rao, etc, "GPS Microstrip Antenna Array on a Resistivity Tapered Ground Plane for Multipath Mitigation". MITRE Corporation

[5] Computational Physics, Inc. "PIM 1.7 User Guide", 13 January 1998.

[6] Davies,Kenneth, "Ionospheric Radio", Peter Peregrinus Ltd., London,1990, p-57.

[7] Dieter Bilitza, "International Reference Ionosphere 2000", Radio Science, Vol. 36, Number 2, Pages 261-275, March-April 2001.

[8] Dr. A. J. Van Dierendonck and Dr. Queyen Hua, "Measuring Ionospheric Scintillation Effects from GPS Signals", GPS Silicon Valley, Los Altos, CA,

[9] Elliott D. Kaplan, "Understanding GPS: Principles and Applications. ", Artech House, Boston, 1996.

[10] GSV GPS Silicon Valley, "GSV 4004 GPS Ionospheric Scintillation and TEC Monitor (GISTM), User's Manual", 22 September, 2001.

[11] H. Socicher and Z. Houminer, "Determination of foF2 short-term variations from GPS time delay observations", Acta Geodaetica et Geophysica Hungaria, Volume 33, number 1, pp 111-119, 1998.

[12] ICD-GPS-200, NAVSTAR GPS Space Segment/Navigation User Interfaces (Public Release Version), ARINC Research Corporation, 11770 Warner Ave., Suite 210, Fountain Valley CA, 92708, July 3, 1991.

[13] J. A. Klobuchar. "Ionospheric Effects on GPS", Chapter 12 in "Global Positioning System: Theory and Applications, Vol 2", edited by, B W and Spilker, J J, Progress in Astronautics and Aeronautics, Vol 164, page 485~515, 1996.

[14] J. E. Allnutt, "Satellite to Ground Radiowave Propagation—Theory, Practice and system impact at frequencies above 1GHz", IEE Electomagnetics Waves Series 29, Peter Peregrinus Ltd, 1990.

[15] NovAtel Inc., "OEM 4 Family of Receivers, User Manual – Volume 1 Installation and Operation", NovAtel Inc., 2001.

[16] NovAtel Inc., "OEM 4 Family of Receivers, User Manual – Volume 2 Command and Log Reference", NovAtel Inc., 2001.

[17] R. E. Daniell, Jr., L. D. Brown, D. N. Anderson, M. W. Fox, P. H. Doherty, D. T. Decker, J. J. Sojka, and R. W. Schunk, "Parameterized ionospheric model: A global ionospheric parameterization based on first principles models", Radio Science, Vol. 30, Number 5, Pages 1499-1510, September-October 1995.

[18] Stefan Schaer, "Mapping and Predicting the Earth's Ionosphere Using the Global Positioning System", Geodätisch-geophysikalische Arbeiten in der Schweiz, v. 59, 1999

[19] T.L. Gulyaeva, "Regional Analytical Model of Ionospheric Total Electron Content: Monthly Mean and Standard Deviation", Radio Science, Vol. 34, Number 6, Pages 1507-1512, November-December 1999.

[20] Topcon Positioning Systems, Inc Online Introduction of "Choke Ring Theory" 2001